UNIVERSITY OF TURKU

A review of machining parameters' influence on surface roughness

Author:
Umer Shaukat

18.11.2024
Turku

Abstract

Manufacturing is essential for modern economics, and machining processes are integral to achieve high quality without forgetting productivity and sustainability in machined components. Surface roughness formed during machining influences the functionality, longevity, reliability, and efficiency of produced parts. Industries like aerospace, medical, and nuclear require high performance components and therefore a more stringent control of surface roughness of machine parts. This study explores the effects of machining process parameters and tool geometry on surface finish. Although, the surface roughness increases with the increasing feed rate and decreases with the increasing cutting speed, the combined interplay between these parameters is highly complex and non-linear. Additionally, increasing the tool nose radius improves the surface roughness. This study develops an ANN model for improving the prediction accuracy of surface roughness at different process conditions. The developed model predicted the surface roughness with an accuracy of nearly 84% and additionally also captured the non-linearity in the machining process efficiently. Furthermore, the accuracy can be improved by employing a hybrid FE-Exp approach to increase the training dataset.

Key words: Turning, machining, surface roughness, surface finish.

Table of contents

Table of figures

1 Introduction

Manufacturing is a cornerstone of modern-day engineering, enabling the transformation of raw materials into functional products. It facilitates the creation of products ranging from mass produced consumer goods to precision engineered aerospace components. Through continuous improvement and integration of advanced technology, it contributes to global industrial competitiveness and national economy. In the United States, manufacturing contributes 20% to the Gross National Product (GNP) and employs 18% of the population [1]. Machining is a vital manufacturing process that involves the controlled removal of material to achieve desired shapes, dimensions, and surface qualities. As a subtractive process, it uses cutting tools to precisely cut the materials. Key machining operations include turning, milling, drilling, and boring. These operations play a crucial role in producing smooth surfaces essential in high precision industries such as aerospace, automotive or powder-based industry, requiring superior surface quality and tight tolerances [2].

Surface quality is usually defined in terms of surface roughness which is a measure of irregularities of a machined surface. It plays a crucial role in determining the functional performance of machined components. A smooth surface reduces friction, improving fatigue resistance and wear performance. While roughness can be occasionally beneficial such as in retaining the lubricating oil between contact surfaces but its disadvantages are far more significant. Rougher surfaces tend to act as stress concentrators, increasing the likelihood of cracking and premature failure under mechanical loads. Surface quality is highly dependent on the process parameters in a machining process. Therefore, optimizing these parameters is essential to achieve desired surface quality.

In a typical machining process, the complex interaction between the cutting tool and the workpiece determines the final characteristics of the machined surface. Cutting tools, commonly made of high strength materials such as carbides, ceramics, or high-speed steels, are typically engineered to withstand substantial cutting forces and temperatures. These tools come in a variety of geometries tailored for specific applications, with each geometrical feature affecting the machining performance and surface finish.

Factors affecting the surface roughness can be categorized into cutting parameters (e.g., feed rate, cutting speed, depth of cut), tool geometry (e.g., rake angle, nose radius) and workpiece material properties (e.g. hardness and thermal conductivity). Cutting parameters significantly affect the surface roughness by influencing the heat flux and force distribution within the cutting

zone while tool parameters determine how a material is sheared, thereby shaping the resulting surface texture. Furthermore, workpiece material properties including hardness, thermal conductivity, and ductility, impact machinability by affecting chip formation. Each of these factors have a distinct effect on the surface finish and texture, either improving or deteriorating the surface quality depending on how the parameters are controlled. This study focuses on developing an ANN model for the prediction of surface roughness based on the machining parameters (specifically turning), tool geometry, and workpiece material. . This study is aimed to develop an ANN model for the prediction of surface roughness using a multi-variable approach. Surface roughness is a critical factor that determines the functional performance of machined components, practically influencing friction, wear, and fatigue life.

1.1 Aims and objectives

As the industries strive for improved performance and cost effectiveness, there is a growing need for optimized machining parameters to achieve desired surface quality with minimum resource use. This requirement is underscored by the increasing demand for high quality and durable parts capable of withstanding rigorous conditions with reduced replacement or maintenance frequency. Optimizing the surface quality enhances the product reliability and minimizes secondary surface finishing needs, decreasing the production needs and making significant contribution to sustainable manufacturing. Traditional empirical models and statistical methods have limitations in effectively capturing multi-object interactions in machining operations. This study uses ANN to predict the surface roughness of machined surfaces using process parameters, tool geometrical factors, and workpiece material. By using a complex dataset, this research seeks to capture complex non-linear interactions between the tool and workpiece, making a step towards reliable and efficient framework for real time roughness prediction, ultimately paving a new road to surface quality control in manufacturing applications.

1.2 Research questions

This study focuses on answering the following research questions:

1. What are the machining parameters that affect the surface roughness with different materials, and how do these parameters interact with the surface quality?
2. How does tool geometry contribute to surface quality in the machining process?

3. How accurately an ANN model predicts the surface roughness based on machining parameters, tool geometry, and workpiece material?

2 Theoretical framework

2.1 Machining

The fundamental process of achieving the final shape and geometry of the material by the removal of the excessive material is named as machining [3]. From industrial perspective, to enhance the profitability and commercialization of a machining process, output variables like surface roughness and product dimensional accuracy are of prime importance [4]. The optimization of any process is done with a compromise between the various process parameters. In machining, the optimization is done by analyzing the effects of selected process variables and tool geometrical parameters on the desired properties like dimensional accuracy, surface finish, energy consumption, production cost, product's fatigue resistance, wear resistance, and tensile strength. Process and parametric optimization lead to improvement in product's cost effectiveness. Other factors of interest in process optimization are build up edge (BUE), tool wear, heat generation, chip formation, cutting forces, power consumption, and vibration level [5–11]. To perform any machining operation, relative motion is required between the tool and workpiece. This motion is achieved by a combination of several elementary motions, such the primary motion, known as the cutting speed, and the secondary motion, known as the feed rate [12]. Turning is a general term used for a group of machining operations in which the workpiece undergoes the primary rotational motion while the cutting insert sweeps across its length. A typical turning process is shown in Figure 1. Three basic surfaces are normally considered in turning:

1. Workpiece surface: This is the surface of the workpiece to be removed by the cutting insert.

2. Machined surface: This is the surface produced after the tool has passed over the workpiece surface.

3. Transient surface: This is the surface being cut by the major cutting edge of the insert.

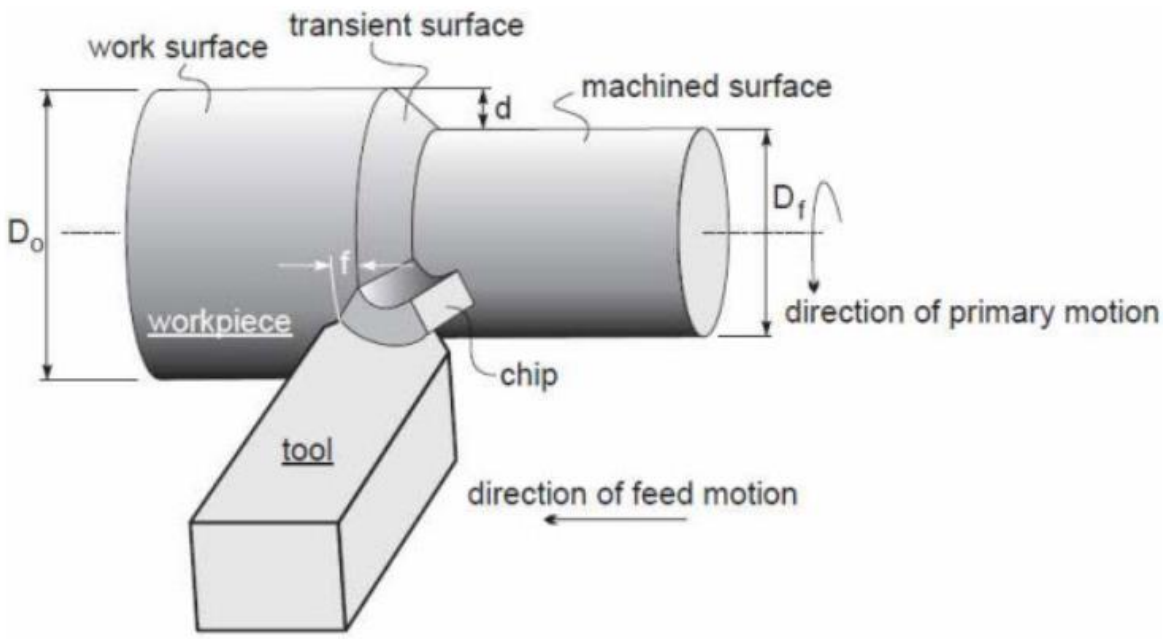

Figure 1: Turning operation [12]

In turning operation, the desired cutting speed is adjusted with the workpiece rotation i.e. the spindle speed (rpm) by taking the workpiece diameter into account. For a workpiece with diameter as 'D' and rotational speed as 'n' rpm, the cutting speed 'v_c' can be calculated as:

$$v_c = \pi D n$$

The feed rate is the distance (along the workpiece length) travelled by the tool during one revolution of the workpiece. In addition to cutting speed and feed rate, there is another parameter named as depth of cut which is simply how deep the cutting insert is into the workpiece. This parameter defines the thickness of the material removed during one revolution of the workpiece. The interaction between the insert and workpiece removes the material from the workpiece. The ease of material removal from a given workpiece during machining is typically defined in terms of material removal rate (MRR). The material removal rate is related to the cutting speed v_c, feed rate f, and depth of cup a_p by the following equation:

$$MRR = v_c f a_p$$

For a given cutting speed and the depth of cutting edge into the workpiece, the tool moves slides over the workpiece from right to the left with a given feed rate.

The cutting insert is made from material which is generally harder than workpiece material. A typical cutting insert in turning operation is shown in Figure 2. Cutting edge interacts with the workpiece to remove the material.

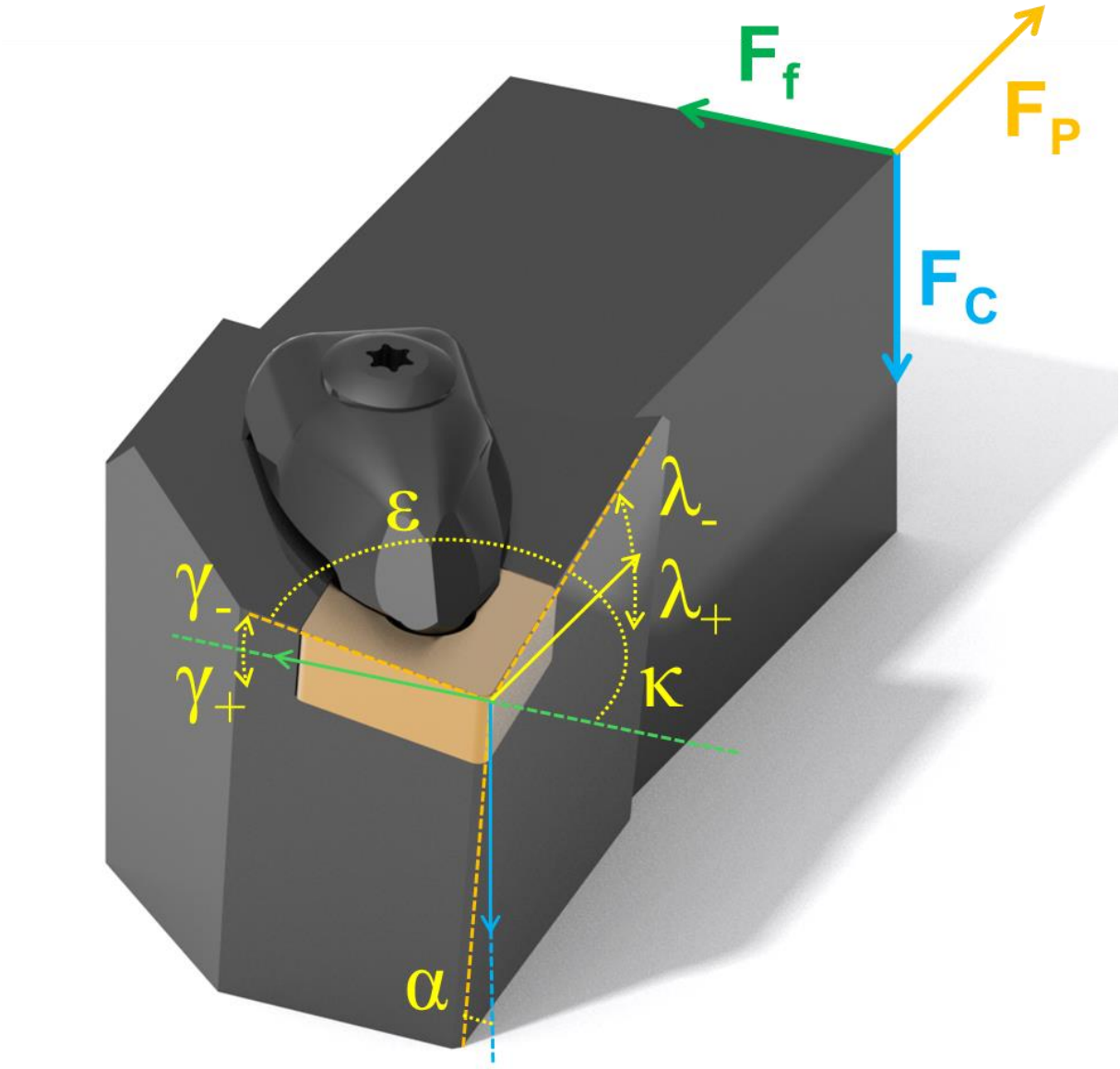

Figure 2: Cutting insert and tool holder [13]

Cutting inserts exist in thousands of shapes, sizes, and material combinations. Each insert is optimized for maximum wear resistance. The material flow direction is perpendicular to the rake face while the chip flow direction is parallel to the rake face. In other words, rake face

directs the flow of chips formed during the machining operation. The cutting inserts can contain a chip breaker to reduce the tool-chip contact length.

There are three zones in a machining process namely as [14]:

1. Primary Zone
2. Secondary Zone
3. Tertiary Zone

The primary zone consists of the main deformation zone between the workpiece and cutting tool. The secondary zone initiates at the boundary between the chip and insert rake face. This zone gives information about the friction between the chip and cutting insert. The third zone, named as the tertiary zone, is at the machining surface i.e. the machined surface obtained and the flank face. This zone provides information about the surface quality of the workpiece after machining.

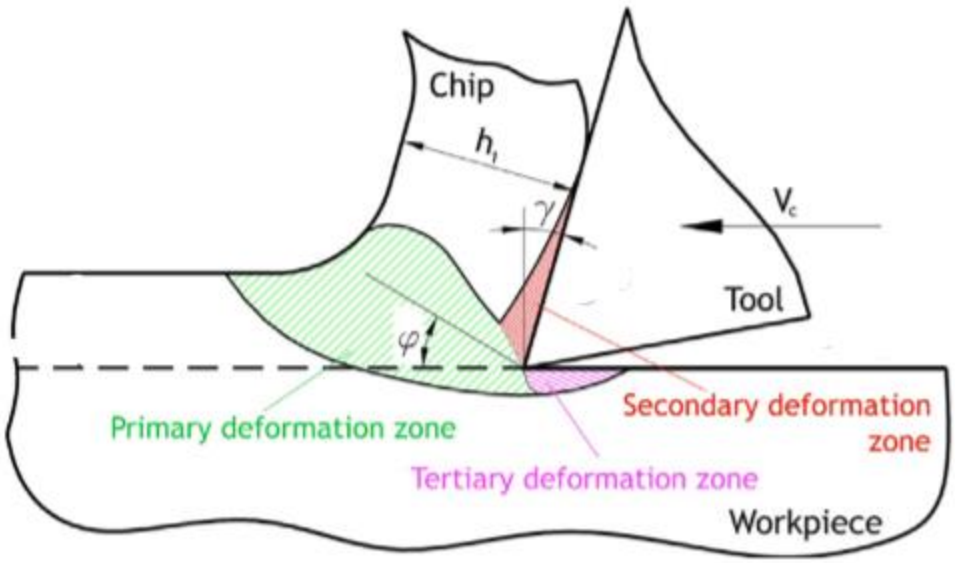

Figure 3: Three deformation zones in machining [15]

While removing the material, the tool applies a certain force on the layer to be removed. This force, commonly known as the resultant cutting force, is a 3D vector considered in a machine reference system according to ISO 841 as shown in Figure 4. Cutting edge serves as the origin of this coordinate system. For convenience, the resultant cutting force is resolved into three components. The main component is the cutting force (F_c) which is normally the greatest

component. The force component in the feed direction is known as the feed force (F_f). The last component which is along the depth of cut is called the radial force (F_r). These forces are responsible for chip formation and material removal from the workpiece [16]. The cutting power (P) used to remove the material removal from the workpiece is normally calculated as:

$$P = F_c . v_c$$

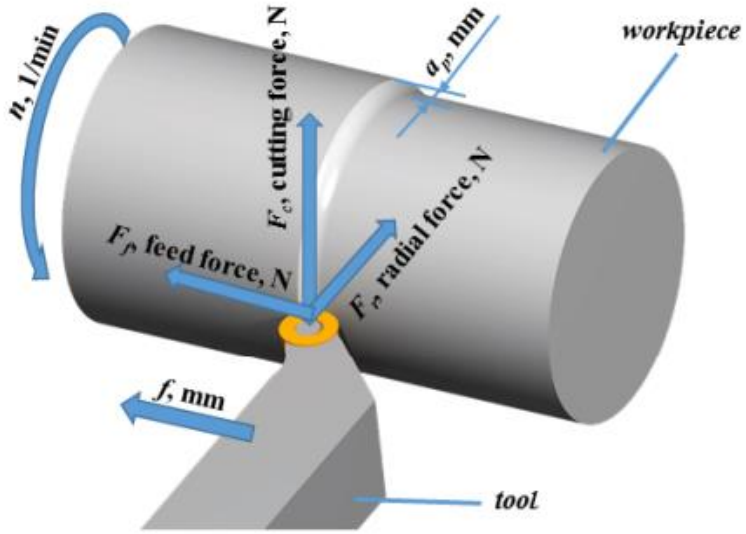

Figure 4: Cutting force and its components as applied to the workpiece [16]

Shear deformation of the workpiece to form the chip is the predominant cutting action in machining. After the chip is formed, the new surface of the material is exposed to the tool. Chip formation takes place along the shear plane oriented at an angle ∅ with the material surface. At the interaction region of the cutting edge and workpiece, the material deforms plastically. Normally, the cutting power is optimized for minimum plastic deformation required for material removal from the workpiece. When such a stage is reached, failure of the material occurs and chip separates from the parent material. Bulk of the energy consumed during the machining process is along the shear plane where the material deforms plastically [3,12].

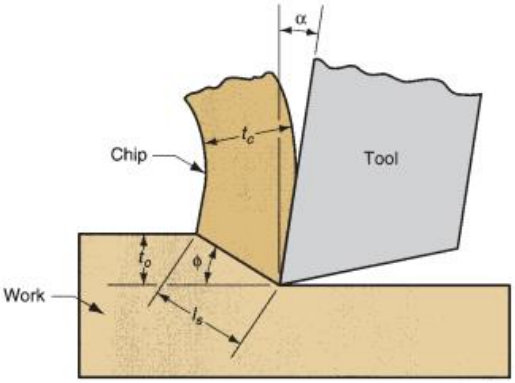

Figure 5: Shear deformation of the material by the cutting tool to form chips [17]

Chip thickness ratio before and after deformation helps to find the shear strain during the machining operation. During the cutting process, the tool is placed at a certain distance below the material's outer surface, known as the undeformed chip thickness 't_o'. After the formation of chips along the shear plane, chip thickness increases to 't_c', known as the deformed chip thickness. The chip thickness ratio of undeformed and deformed chips is written as:

$$r = \frac{t_o}{t_c}$$

The tool used in metal cutting has two main geometry elements namely: rake angle and clearance angle. Rake angle 'α' as depicted in Figure 6, gives the chip flow direction, whereas the clearance angle provides clearance between the flank and newly formed work surface. The shearing of workpiece forms chips and each chip forms a shear plate. From the geometry of machining model shown in Figure 6, the shear orientation comes out to be [18]:

$$\tan \emptyset = \frac{l_s \sin \emptyset}{l_s \cos(\emptyset - \alpha)} = \frac{r \cos \alpha}{1 - r \sin \alpha}$$

The shear strain can be written as:

$$\gamma = \tan(\emptyset - \alpha) + \cot \emptyset$$

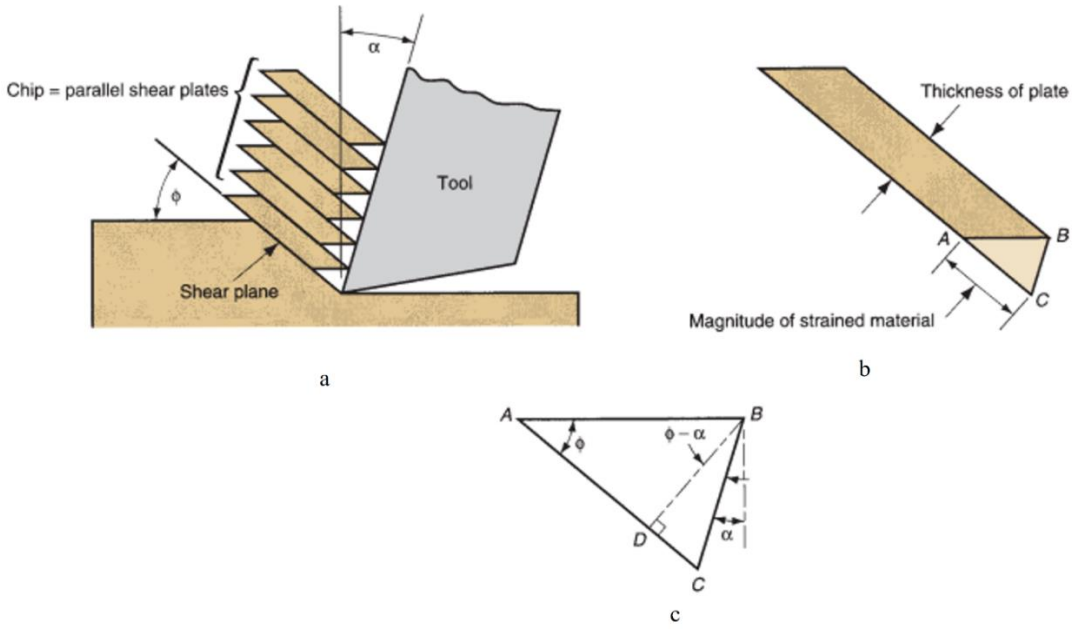

Figure 6: Shear deformation geometry by the cutting tool to form chips (a) Chip formation and shear plane (b) Deformed material segment (c) Shear angle geometry [17]

Primary shear zone is primarily very thin [19]. In three-dimensional models, a second phenomenon happens in the chip after its formation due to the friction which occurs as the chips slide over the rake face.

Chip formation is influenced by cutting conditions and type of workpiece material. When brittle materials are machined at low cutting speed, they form discontinuous chips as shown in Figure 7(a). This is primarily due to high tool-workpiece friction and larger feed rates leading to the formation of an irregular machined surface. In contrast, when a ductile material is machined at relatively higher speed and lower feed rate, continuous chips are formed, producing a good surface finish [Figure 7(b)]. However, at lower speeds, the cutting temperature is too low, causing adhesion of the machined surface material with the tool, leading to the formation of built-up edge (BUE) [Figure 7 (c)]. While BUE generally detaches from the tool during the chip separation, it can also remove small portion of the tool material, accelerating tool wear and increasing surface roughness [20]. Machining difficult-to-cut machine materials like titanium alloys, nickel super alloys, and austenitic forms saw-tooth chips. These semi-continuous chips are called serrated chips depicted in Figure 7(d) [17].

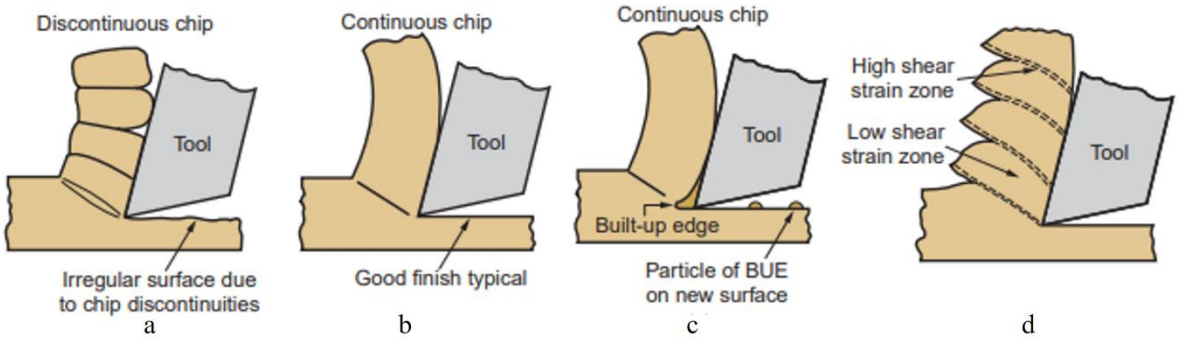

Figure 7: Various chip types formed during machining (a) Discontinuous (b) Continuous (c) Continuous chip with built-up edge (BUE) (d) Serrated [17]

The friction between the tool and the chips converts 98% of the total energy consumption during the machining process to heat. When the chips are separated from the workpiece, a portion of the heat also moves away with the chips, making the workpiece less susceptible to heat generated issues. Contrarily tools are majorly affected. Cutting temperatures can reach over 600°C during machining. High cutting temperatures reduce tool life and hot chips pose hazards to machine operators. Several studies have been conducted to calculate the cutting temperature during machining operation [17,21–24]. Jaeger et al. [25] provided a foundation for machining temperature analysis by analyzing the temperature rise due to a rectangular or band shaped heat source sliding at a constant velocity over a semi-indefinite solid. The steady state temperature at the tool-chip interface was given by:

$$T = \frac{0.946 * q * l}{K_1 + 1.388 * (l * K_2 * c)^{0.5}}$$

where T is the average interface temperature, q is the heat generated per unit area, l is the effective length of the heat source (contact area between the tool and chip), K_1, K_2 are thermal conductivities of workpiece and tool, respectively, and c is the specific heat capacity of the workpiece. While this model provided the foundation for analysing moving heat sources, it had several limitations. This model assumed uniform heat flux over a rectangular surface, whereas real machining involves non-uniform heating due to discontinuous and non-uniform tool-chip interaction. Additionally, transient effects were also neglected and effect of cutting fluids was completely ignored [25].

This model was refined by Chao and Trigger [24] by accounting for the three heat source primary shear zone, secondary zone, and tertiary zone. The temperature at the tool-chip interface was estimated by:

$$T = A * F_c * v_c * (1 - B_1) - F_f * v_c * a_v + \left(\frac{B_2}{9.5\pi^{0.5}}\right) * \frac{F_T}{K l_c} * \left(\frac{k * v_c * a_v}{b}\right)^{0.5}$$

where A is proportion of mechanical energy that converts into heat and raises temperature, F_c is the cutting force, v_c is cutting speed B_1 is the proportion of heat flowing from the shear plane to the workpiece F_f is the thrust force a_v is the exit speed of the chip, q is the chip material density, c is the chip material specific heat, b is the cutting width, f is the feed, B_2 is the proportion of heat that flows from the chip/tool interface to the chip, F_T is the projection of the main cutting force on the rake face in the tangential direction, k is the thermal diffusivity, K is the thermal conductivity, l_c is the chip-tool contact length on the rake face. This model was based on uniform heat distribution, differing from the practical machining operation [24]. Later, Cook et. al [22] modified Jaeger's model by incorporating temperature dependent material properties, considering heat partition between tool, chip, and workpiece, and accounting for the changes in thermal properties of the involved materials due to high strain rate and plastic deformation. Cook et al. derived the temperature equation at the tool chip interface using the experimental data. The equation for the prediction of temperature is as follows:

$$\Delta T = \frac{0.4U}{\rho C}\left(\frac{v t_o}{K}\right)^{0.333}$$

where U is the specific energy during the operation, ρC is volumetric specific heat, and K is the thermal diffusivity of the workpiece.

Trigger et al. [26], experimentally, developed the relationship between the tool-chip interface temperature and cutting speed using a tool-chip thermocouple:

$$T = K v^m$$

where K and m are dependent on the cutting conditions and work material. This model was material specific, and it ignores the heat partitioning between tool, chip, and workpiece.

Recent advancements in temperature modelling in turning operation have improved accuracy by incorporating material specific thermal properties. Liu et al. [27] developed an empirical model, describing the heat transfer coefficient as:

$$h = 277.52 * {v_c}^{0.1112} * f^{0.0940} * {K_{eq}}^{0.0062}$$

where h is the heat transfer coefficient, v_c is the cutting speed, f is the feed rate, and K_{eq} is the equivalent thermal conductivity of the cutting material. This model was validated experimentally for compacted graphite iron, showing improved accuracy over earlier empirical formulations. The incorporation of K_{eq} accounts for workpiece material and tool coatings making it more robust for practical applications. The suggestion of incorporating material dependent thermal properties provides a promising approach for developing generalized models. However, this model was approximated for orthotropic hexahedron tool shapes. The potential for analytical models is always high considering that their solution needs lower computational power. But, numerical models remain an accurate approach for scenarios considering detailed geometrical requirements [27]. Although newer models provide results with reasonable accuracy, but finite element method (FEM) is believed to provide more accurate predictions by solving complex heat transfer problems.

As the cutting proceeds in turning operation, various wear mechanisms result in increasing the tool wear. General tool wear as a function of cutting time is plotted in Figure 8.

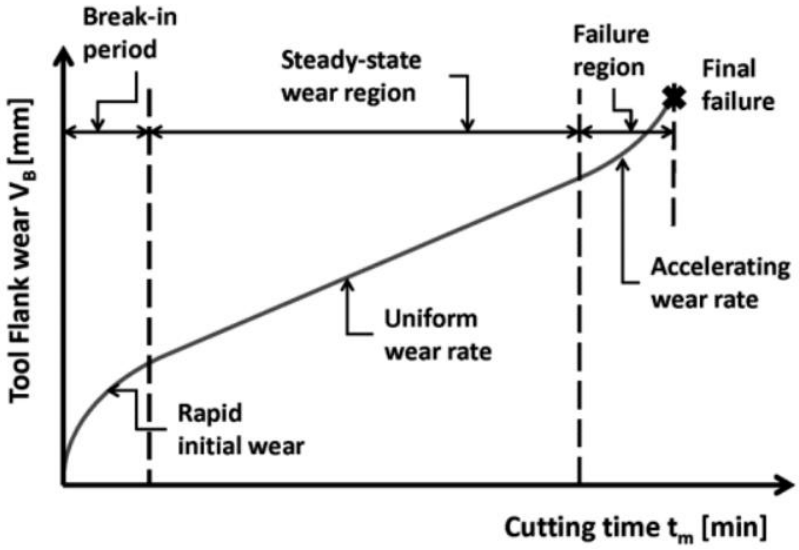

Figure 8: Tool wear as a function of cutting time [28]

Three regions appear in tool's wear growth curve. During the break-in period, the tool initially interacts with the workpiece material, leading to a rapid increase in the tool wear takes due to friction. This is the region within the first few minutes of cutting. The second region is the steady state wear region in which the wear rate is uniform and progresses linearly over time. After this, when the wear rate accelerates rapidly, marking the final failure stage. In this region, cutting temperatures rise significantly, friction increases, and machining efficiency declines, ultimately leading to tool failure. Understanding these wear stages is essential for optimizing machining conditions and maximizing tool life.

The most important factors affecting tool life are toughness, hot hardness, and wear resistance. Toughness is essential to allow the tool to absorb high amounts of energy without failure, ensuring durability during machining. Hot hardness refers to the ability of the tool to retain its hardness at elevated temperature. This is the most crucial factor as it directly affects tool's wear resistance. As shown in Figure 9, tool hardness decreases with increasing temperatures, making the tool softer and more prone to wear and failure. Maintaining high hot hardness is vital for extending tool life and ensuring consistent machining performance.

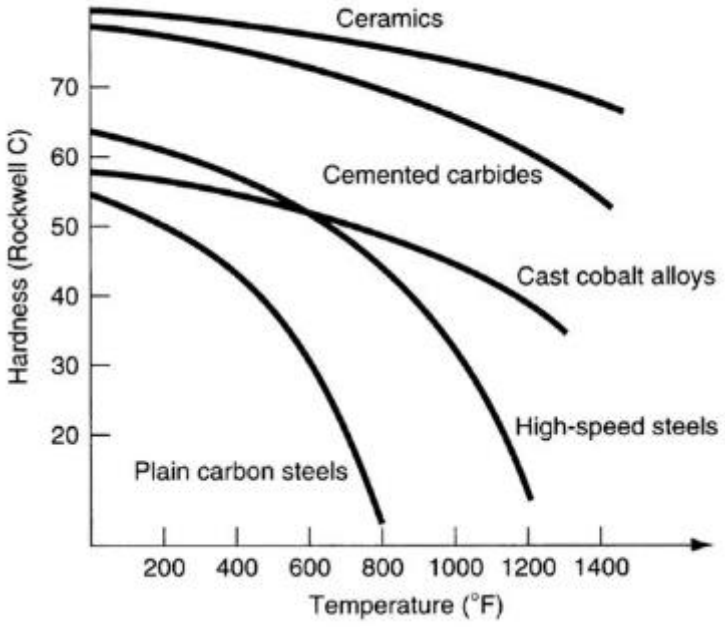

Figure 9: Tool hardness as a function of temperature [29]

In the turning operation, the irregularities in the machined surfaces are inevitable. These discrepancies are caused by both controllable and uncontrollable factors. The components of surface roughness of a machined surface are shown in Figure 10.

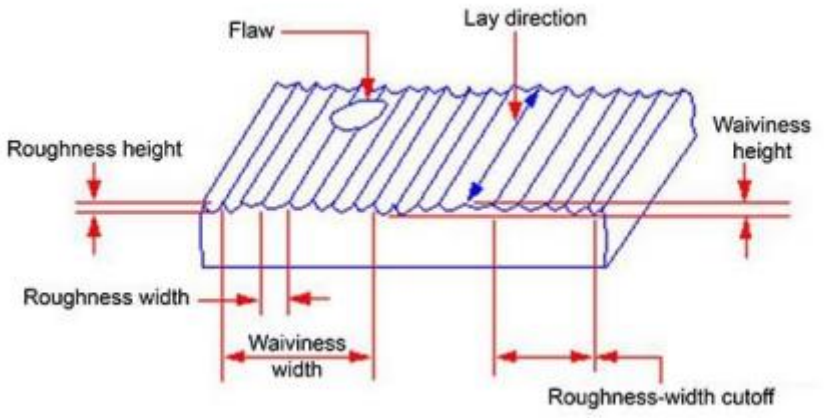

Figure 10: Components of surface roughness [30]

- Surface texture refers to the deviation pattern on a machined surface and is characterized by various parameters that define surface topography like roughness, waviness, lay, and flaws.
- Surface roughness defines the fine irregularities on a machined surface due to the interaction of cutting tool with the workpiece material.
- The average deviation from the mean plane of the machined surface is defined by roughness height.
- The distance between two successive peaks or valleys is termed as roughness width.
- A broader range of irregularities in the machined surface is classified as roughness width cut-off.
- Waviness results from machine vibrations or chatter that leads to larger irregularities spanning across the roughness profile. It is measured over a greater sample length than surface roughness.
- Waviness height is the vertical distance between peek and valleys.
- Waviness width is the spacing between wave peaks or valleys.

- Lay refers to the predominant direction of pattern or irregularity on the machined surface, regardless of roughness or waviness.
- Flaws are unintended imperfection disrupting the expected texture of the machined surface [30].

Surface finish of a machined surface greatly depends on the tool geometrical factors. One of the most influential geometrical parameters is the insert's nose radius. The effect of nose radius on the workpiece roughness is shown in Figure 11.

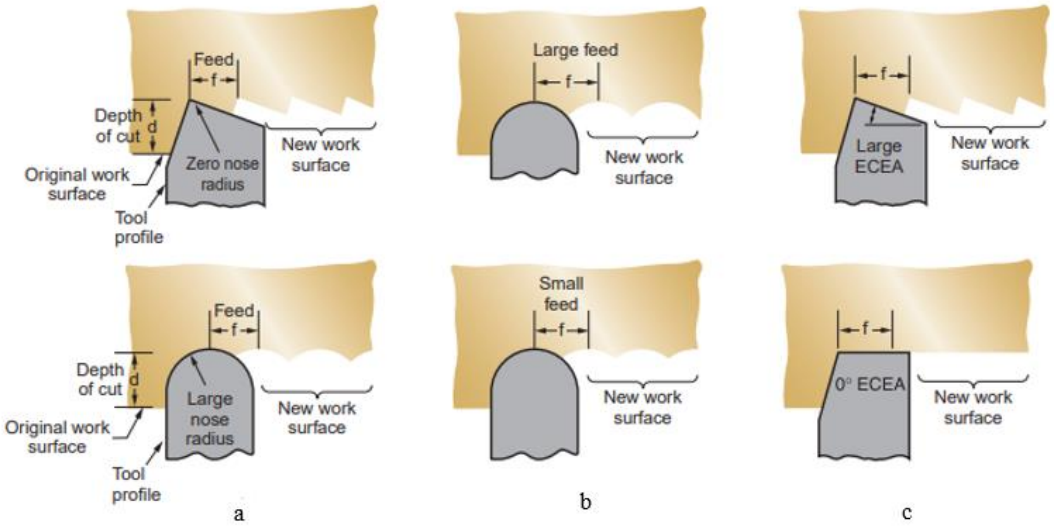

Figure 11: Surface roughness variation with respect to tool nose radius [17]

For the same feed rate, feed marks of the machined surface are less visible for a tool with larger nose radius. Conversely, for same nose radius, increasing the feed negatively affects the roughness of the machined surface. An ideal surface roughness can be achieved by optimizing feed rate and nose radius. For a larger feed rate, if the nose radius is nearly zero, the end cutting edge angle (ECEA) defines the final surface finish. Decreasing ECEA theoretically leads to improved surface quality as depicted in Figure 11Figure 13(c).

Various cases of possible feed marks on the machine surface due to tool nose radius were studied by Vajpayee [31], analyzing the effect of nose radius and feed rate on surface roughness. He developed an accurate analytical formulation:

$$R_i = r_n - \left({r_n}^2 - \frac{f^2}{4} \right)^{1/2}$$

Since the nose radius is generally small (0.2-1.6 mm), the squared radius parameter would reduce further and lead to the following approximation:

$$R_i = \frac{f^2}{8\, r_n}$$

where R_i is the surface roughness, f is the feed rate, and r_n is the tool nose radius. The error between the two equations can be visualized in Figure 12.

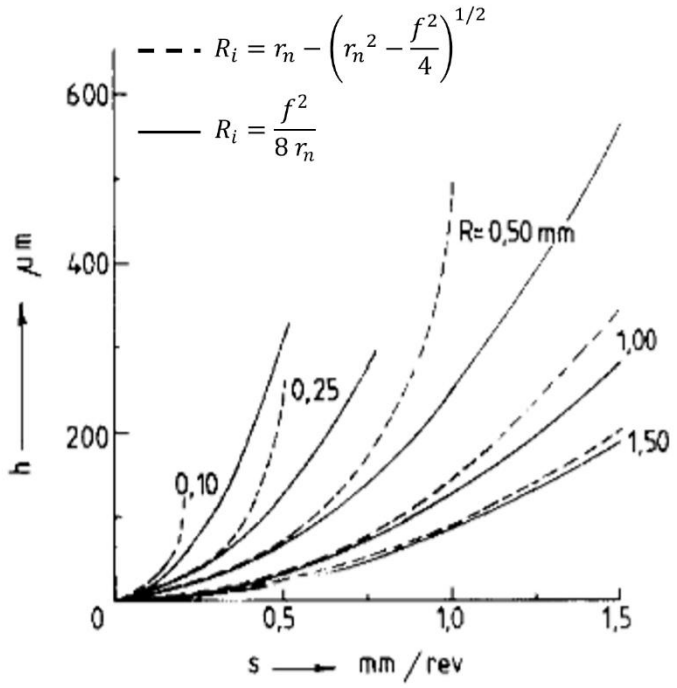

Figure 12: Effect of feed rate and nose radius on surface roughness [31]

For sharp cutting tools, the surface finish is excellent. However, as the machining progresses and the temperature of the tool rises, tool wear becomes significant, leading to deterioration in surface quality.

Achieving an ideal surface finish is inherently challenging due to the variation of factors related to workpiece material and its interaction with the tool. One of the most influential factors in this regard is BUE formation. Cyclic accumulation and breakage of BUE particles results in their deposition onto the machined surface, increasing the surface roughness and creating a sandpaper-like texture. Another prominent factor is chip curling, where chips bending back onto the workpiece comprise the surface finish. Depending on the cutting condition, chips exhibit various tearing patterns like continuous, discontinuous, and serrated. Discontinuous

chips specifically lead to the formation of cracks on the machined surface. Friction between the tool and the chips plays a crucial role in determining the surface roughness. All these factors are strongly influenced by machining parameters. The ratio of actual to ideal surface roughness decreases as the cutting speed increases as illustrated in Figure 13.

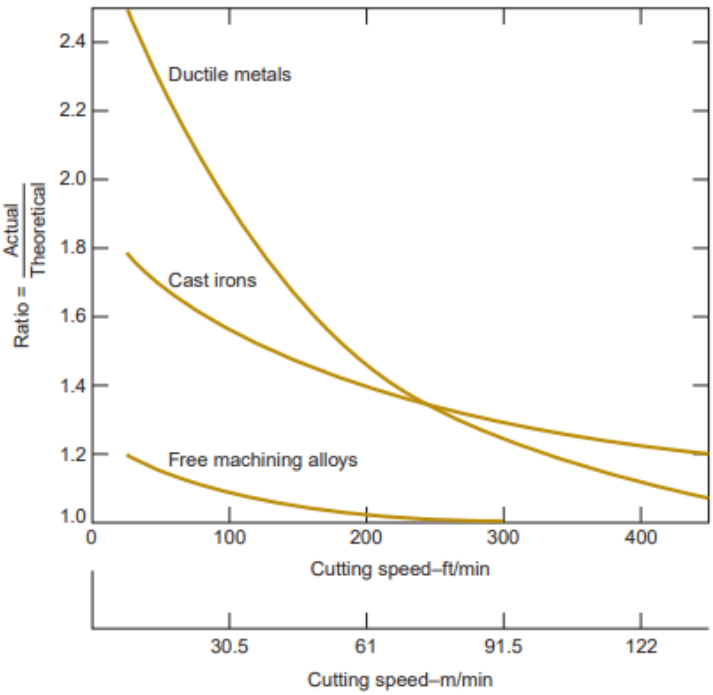

Figure 13: Actual to ideal surface roughness ratio with respect to cutting speed [17]

2.2 Machine learning

Conventional methods in machining context are established on a physical model aiming to extrapolate the correlations between the model variables. Such models are often analytical and give poor generalization of process non-linearity. Contrarily, the purpose of machine learning (ML) is to obtain an accurate predictor that can recognize complex patterns in the data which are impossible to be incorporated into analytical models. ML, itself is a subset of artificial intelligence (AI), and it enables a computer or machine system to learn from experience [32].

The integration of ML and AI is driving the revolution in machining processes towards industry 4.0, characterized by interconnected systems and smart factories. Researchers are using AI systems to optimize machining parameters in real time to enhance product quality and operational efficiency [33].

ML architecture is classified as supervised, unsupervised, and reinforced learning. Supervised learning is employed where input and output datasets are available, and the forecast outcomes of the model need to be verified with real resultant datasets. In unsupervised learning the input dataset is available without any knowledge about the possible outcomes. This modelling technique has been implemented to improve the time-consuming limitations in supervised learning. Reinforced learning is based on reward and penalty system in which the model gets a reward when it accurately predicts the outcome and gets penalized when it is wrong, enabling it to improve continuously [34].

There are various ML and AI based algorithms. For instance, artificial neural networks (ANNs) are computational AI models inspired by the human brain, capable of capturing nonlinear relationships within the given dataset. Deep Learning, a subset of ML, uses multiple layers to optimize models for intricate data patterns. Convolutional neural networks (CNNs) are specialized for spatial data recognition. These models are employed for surface roughness prediction by analyzing machined surface images. Long short term memory (LSTM), a type of recurrent neural network (RNN) are adept in modelling temporal patterns in machining processes [35].

The intricate influence of machining parameters like cutting speed, feed rate, depth of cut, tool nose radius, material specific properties, friction, heat flux etc. on surface roughness makes ANNs well-suited to model the process non-linearity. ANNs can effectively learn from empirical data to predict surface roughness with high accuracy. ANN's architecture comprises of three components:

1. Input layer
2. Hidden layer
3. Output layer

Input layer is the initial interface of ANN where the external dataset is introduced into the model. This layer consists of several nodes with each node representing a specific feature from the given dataset. In this way, the input layer acts as a conduit to pass the raw information to subsequent layers.

Hidden layers are positioned between the input and output layer and are pivotal in the model's ability to learn from the given dataset. Each hidden layer consists of several neurons, applying

specific transformations to the input features. These transformations are performed with the help of weight computations. Each neuron computes a weight sum of the input features from the previous layer as follows:

$$z_j = \sum_{i=1}^{n} w_{ji} x_i + b_j$$

where z_j is the net input to neuron j, x_i is the input form neuron i of the previous layer, w_{ji} is the weight assigned to the connection between the neuron i and j, b_j is the bias, and n is the number of neurons .

For each neuron, the weighted sum is passed through an activation function to introduce non-linearity. The architecture of a single neuron is illustrated in Figure 14 [36].

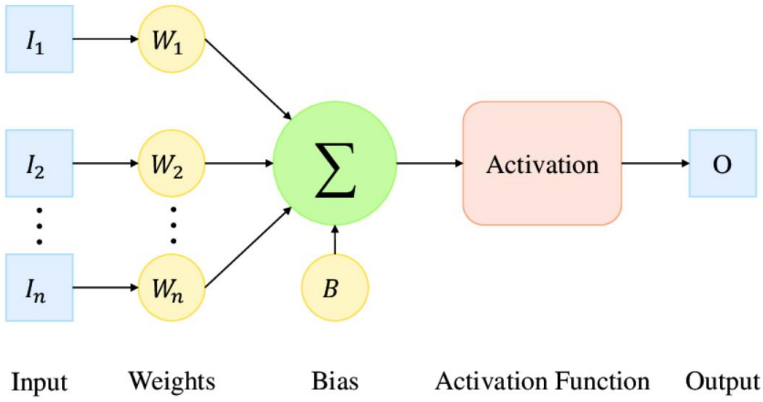

Figure 14: Single neuron architecture [36]

Activation functions enable ANNs to learn the complex interdependencies and patterns in the input features. Without any activation functions ANNs would behave as linear regression which is a type of supervised learning. Different activation functions for an ANN model are shown in Figure 16. The Sigmoid function is used for binary classification tasks and is particularly for probability-based interpretations. Hyperbolic tangent function is used in deep neural networks where data needs to be centered around zero. This function is well suited for natural language processing (NLP) models. The reactive linear unit (ReLU) function is used in deep learning models where it is necessary to capture non-linear relationships. Leaky ReLU is used to avoid the dying ReLU problem which arises when the neurons start giving zero output [37].

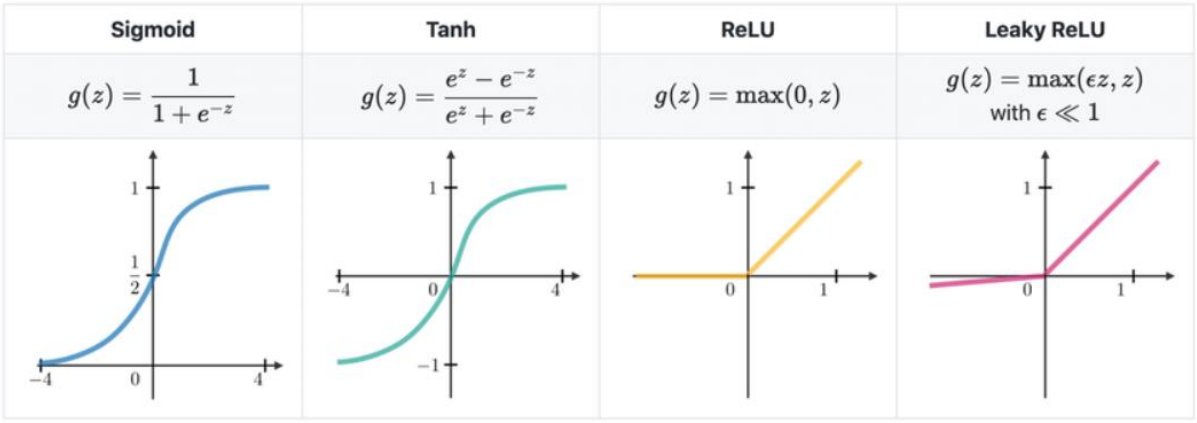

Figure 15: ANN model architecture [37]

ANN models rely on loss functions to quantify the difference between predicted output and actual output values, enabling the model to assess its accuracy during training. To minimize the error, ANNs utilize backpropagation, a learning model that applied a chain rule for gradients calculations. This approach systematically adjusts the weights for each neuron, iteratively improving the model's performance [38].

Optimizers are crucial components in this process, as they determine how the weights are updated to minimize the loss function. Stochastic gradient descent and Adam optimizer are two optimization algorithms developed to accelerate the convergence of neural networks.

Stochastic gradient descent updates weights after processing each training sample, leading to fluctuations in the optimization path. Contrarily, Adam optimizer reduces these fluctuations by combining momentum based learning and adaptive learning rates to optimize the ANN efficiency [39].

Once the ANN model is trained, it makes predictions based on the optimized weights and biases. The final output is computer as:

$$\hat{y} = f\left(\sum_{i=1}^{n} w_i x_i + b\right)$$

where f is the activation function, w_i is, the trained weight, x_i are the input features, and b is the bias term. The complete architecture of an ANN model is shown in Figure 16

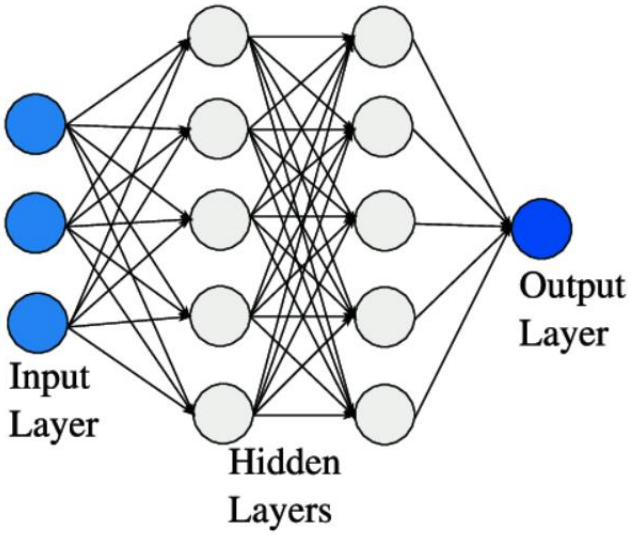

Figure 16: ANN model architecture [40]

3 Literature review

Surface roughness is a critical factor in machining, directly influencing product quality, durability, and performance. It plays a vital role in determining the functional characteristics of machined components, affecting their fatigue life, wear resistance, and tribological behavior. Researchers have extensively studied the effect of machining parameters like feed rate, cutting speed, depth of cut, tool geometry, lubrication, and workpiece material properties. The interaction between these parameters determines the final surface finish, making their optimization essential in machining research.

A deep understanding of surface roughness is crucial for enhancing manufacturing efficiency and ensuring product reliability. Elevated roughness levels can lead to stress concentration, increasing the likelihood of premature failure, while an excessively smooth surface may escalate production costs without any significant functional advantages. Therefore, choosing optimal machining parameters is a trade-off between surface quality and production efficiency. This review focuses on investigating the influence of process parameters on surface roughness in machining operation. Numerous studies have confirmed that the feed rate has the most significant impact on surface roughness, in comparison to cutting speed and depth of cut. Higher feed rates generally lead to increased surface roughness due to larger uncut chip thickness. Rusdi et al. [41] found that feed rate was inversely related to surface finish while cutting speed had no significant effect on surface roughness. Qehaja et al. [42] confirmed these results and demonstrated that an increased depth accelerates tool wear, indirectly increasing surface roughness. Kumar et al. [43] optimized the material removal rate (MRR) for AISI 321 stainless steel using Taguchi's methodology and concluded that depth of cut was the most influential parameter on MRR. Several other researchers [44] concluded similar results that feed rate has the high influence, affecting both surface roughness and dimensional inaccuracy, while cutting speed moderately improved the surface finish.

Wu and Lin [45] and Srivastava et al. [46] reviewed the effect of depth of cut on surface roughness. Their studies found that the depth of cut had the least contributions to surface deviations, but high values led to an improved material removal rate due to thermal softening.

3.1 Effect of tool geometry

Tool geometrical parameters including nose radius, rake angle, and clearance angle, play a critical role in determining surface roughness. The relationship between the tool nose radius and surface roughness was first established by Albrecht et al. [47], highlighting its effect on surface quality. Thiele et al. [48] studied the hard turning of AISI 51200 and found that increasing the tool nose radius elevates the roughness levels due to increased heat generation and plastic deformation. On the other hand, Childs et al. [49,50] concluded that in conventional machining, machine tool errors had a greater influence on surface finish than tool nose radius.

Daniyan et al. [51] examined the effect of tool nose radius and rake angle in the milling of Ti6Al4V titanium alloy of surface roughness, using computer aided modelling and experimental validation. The findings revealed that larger tool nose radii stabilized the cutting process and improved surface finish. However, excessively large nose radius led to increased heat generation, causing tool wear and material adhesion. Positive rake angles improved surface roughness by reducing cutting forces, whereas negative rake angles increased the machining resistance and led to an increase in surface roughness. This was confirmed by Saravanamurugan et al. [52] using finite element method (FEA) and response surface methodology (RSM).

Bhushan [53], Kumar et al. [54], and Niu et al. [55] also confirmed the improvement of surface quality with increasing nose radius. However, Kumar et al. [54] found that when the nose radius was increased from 0.4 mm to 0.8 mm, the cutting forces increased by 2-3 times.

Wang et al. [56] used molecular dynamics (MD) simulations to analyze effects of machining parameters in nano-cutting of tungsten and found that larger rake angles and clearance angles resulted in reduced cutting force, cutting temperature, and friction coefficient, improving surface finish and elastic recovery. Smaller edge radii minimized subsurface damage and decreased residual stresses and plastic deformation.

Hence, positive rake angles facilitate chip evacuation and reduce surface roughness. Additionally, larger nose radii enhance surface finish but increase cutting forces due to higher tool-workpiece contact area. Clearance angles contribute to vibration control, tool wear reduction, and surface integrity.

3.2 Influence of lubrication and machining environment

Lubrication conditions significantly impact surface roughness by influencing friction, heat dissipation, and tool wear. Sreejith [57] compared dry, wet, and minimum quantity lubrication (MQL) conditions, concluding that MQL provided an optimal balance between efficiency and sustainability, reducing surface roughness more effectively than dry machining. Kamata and Obikawa [58] and Khan et al. [59] also confirmed that MQL improved surface roughness in machining Inconel 718 and AISI 9130 steel, while Javidikia et al. [60] demonstrated that wet machining and MQL achieved superior surface finish compared to dry machining. Gupta et al. [61] studied the effect of dual-jet MQL in turning duplex stainless steel and found that lubrication applied to both flank and rake faces reduced surface roughness by 25% in comparison to single jet MQL. Shinge & Pable [62] and Kumari et al. [63] tried to improve the process using nano-MQL (nMQL), and they found that surface roughness was reduced by 40%. Zhang et al. [64] took another step ahead and investigated the effect of cryogenic cooling. They found that it produced better surface finish in comparison MQL. Similar results were obtained by Ünal Değirmenci et al. [65]. Şap et al. [66] studied the effect of liquid nitrogen (LN_2) on surface roughness, and concluded that the roughness increased due to increased dislocation density and work hardening. However, Chauhan et al. [67] found that while using cryogenic cooling, power consumption increases by 6% - 28%. Singh and Sharma [68] demonstrated that surface finish can be improved further using ultrasonically atomized fluid (UAF) but this also increased the airborne particles, potentially enhancing the vulnerability to respiratory problems. Mohd Danish et al. [69] and Kumari et al. [63] devised a hybrid cryo-MQL and achieved lowest surface roughness while balancing cooling and lubrication effects, demonstrating super thermal stability and reduced tool wear. To make the process more cost effective, Liu et al. [70] found that cold air electrostatic MQL (CAEMQL) improved fluid penetration and cooling efficiency, improving the surface quality.

These studies confirmed that lubrication conditions are crucial in determining surface roughness, with MQL and hybrid Cryo-MQL proving the most effective. Cryogenic cooling improves thermal stability but suffered due to work hardening effects, while nMQL achieved superior lubrication and roughness reduction. CAEMQL achieved similar surface quality while optimizing the process economics. Selecting an appropriate lubrication strategy can significantly improve machining performance, surface integrity, and tool life, making advanced lubrication techniques essential for improving surface integrity.

3.3 AI-driven approaches in surface roughness prediction

Despite the recent advancements in process optimization in machining, predicting the final properties of the product based on the process parameters is still challenging. AI and ML have transformed rough prediction by capturing complex interactions between the machine, tool, and workpiece that are difficult to address with traditional models. ANNs, support vector machines (SVMs), random forest (RF), and deep learning models like convolutional neural networks (CNNs) leverage machining parameters, sensor data, and advanced image processing techniques to improve the prediction accuracy. These data-driven approaches enable real-time monitoring and optimization, enhancing machining efficiency and surface quality [71].

Yang et al. [72] demonstrated that CNNs outperform traditional models in roughness prediction, but suffer from extensive data requirements, poor generalization, and high computational costs. Motta et al. [73] employed RF and gaussian process regression (GPR) for roughness prediction. GPR achieved a root mean square error (RMSE) of less than 0.4 µm, but the model struggled with varying roughness levels, severely affecting its generalization ability. Mazid et al. [74] applied SVM, RF, and deep learning to for surface roughness prediction in machining and found that SVM demonstrated the best performance but it also lacked generalizability due to limited dataset. Eser et al. [75] also found similar results. Ross et al. [76] took a step further and introduced transformers based generative adversarial networks (TransGAN) for data augmentation and used a multi-head attention (MHA) based model for roughness prediction. Model dependence on image-based classification techniques restricted its precision in machining applications. Among different AI models, ANNs have consistently demonstrated higher accuracy in capturing nonlinear machining behaviors. Huang et al. [77] developed an ANN based model for roughness prediction across multiple materials and achieved an accuracy of nearly 97%, surpassing single material models. This model demonstrated a good capability to generalize the results for different materials and different machining conditions, reinforcing its superiority over other models.

4 Materials and methods

The ANN model developed in this work is based on two turning experiments carried out on two different materials i.e. 42CrMo4 alloy steel (AISI 4140) and Aluminum 2014 (Al-2014). The first study was done by Laakso et al. [78] and it focused on the evaluation of surface roughness in turning on AISI 4140 using a Daewoo Puma MX2500 ST CNC lathe, a 9-axis machine equipped with a 380 mm chuck size and a 26 kW spindle motor, capable of reaching 3500 RPM. The workpiece material was provided by Ovako, having a diameter of 120 mm and length of 300 mm. The material was quenched and tempered which resulted in a hardness of 300 HV. This was verified using a Struers polishing machine before the machining operation. The experimental setup on the CNC is shown in Figure 17.

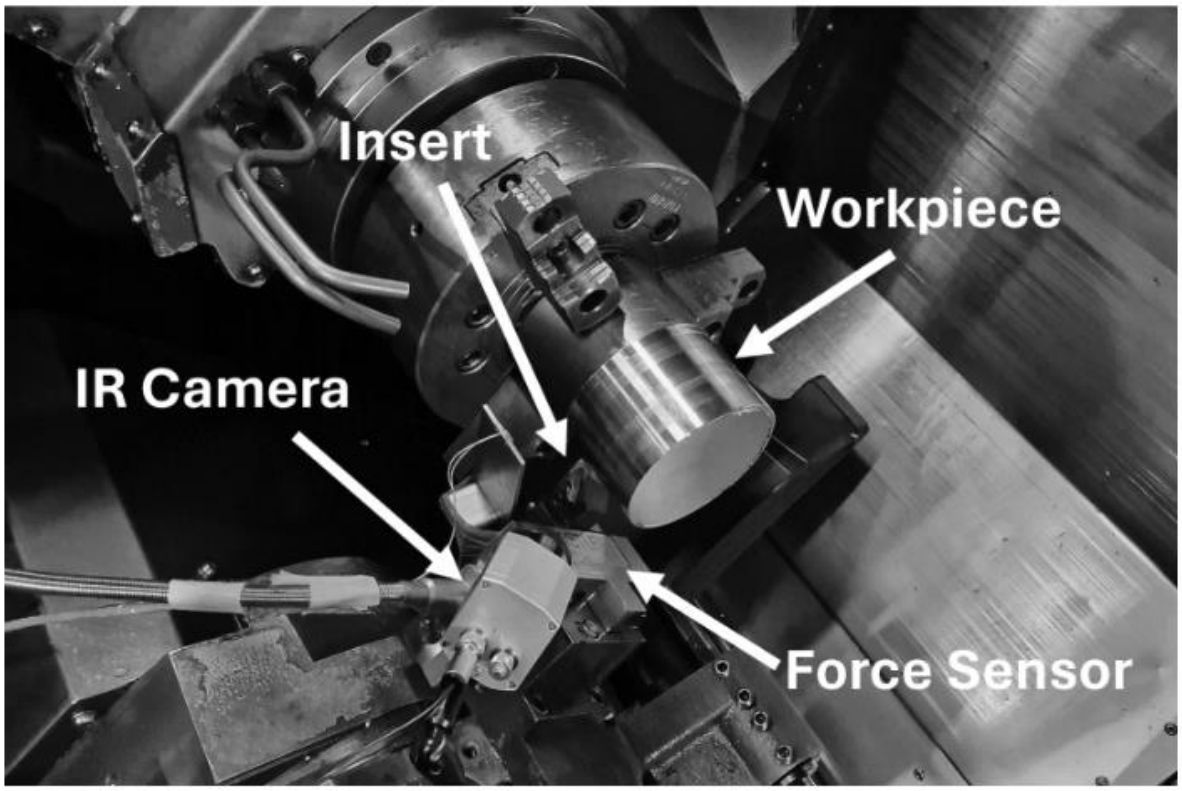

Figure 17: Experimental setup for turning of 42CrMo4 (AISI 4140) [78]

A seco tools CNGA120408S-01525-L1-B CH2540 CBN insert was used for turning, mounted on a DCLNR2525M12-M tool holder. The reason for choosing this insert was its high hardness and wear resistance, theoretically depicting the potential of providing a consistent surface finish during machining. Table 1 shows the geometrical properties of the insert.

Table 1: Geometrical properties of CBN insert

Parameter	**Value**
Nose radius (r_n)	0.8 mm
Rake angle (γ)	-6.0°
Major cutting-edge angle (κ)	95.0°
Inclination angle (λ)	-6.0°
Included angle (ε)	80.0°

Repeatability and statistical validation of the results was ensured by selecting the cutting parameters using a two-level full factorial experimental design with center points. Nine cutting conditions were tested, where cutting speed (v_c) varied from 135 to 225 m/min, feed rate (f) from 0.075 to 0.125 mm/rev, and depth of cut (a_p) from 0.3 to 0.5 mm as given in

Table 2. The surface roughness was measured using Alicona Infinite Focus G6 shown in Figure 18.

Table 2: Design of experiments [78]

Test ID	**v_c (m/min)**	**f (mm/rev)**	**a_p (mm)**
A	225	0.125	0.5
B	135	0.125	0.5
C	225	0.075	0.5
D	135	0.075	0.5
E	180	0.1	0.4
F	225	0.125	0.3
G	135	0.125	0.3
H	225	0.075	0.3
I	135	0.075	0.3

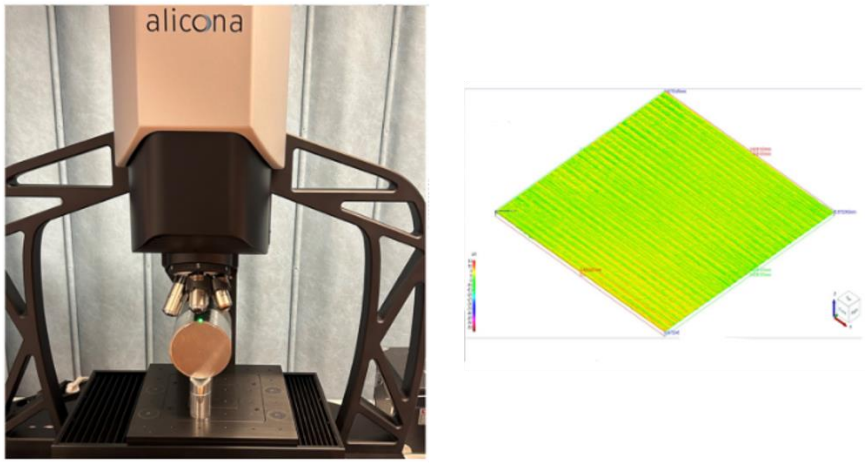

(a) (b)

Figure 18: (a) Alicona Infinite Focus G6 microscope (b) Surface Topography

The second study was carried out by Shaukat et al. [79] which utilized a YIDA ML-300 CNC machine. A bar of aluminum 2014 (Al-2014), having a diameter of 160 mm and length of 300 mm was machined using an uncoated insert CCMW-09 T3 03-H13A ($r_n = 0.387$ mm) provided by Sandvik Coromant. to develop optimized surface roughness maps. The experimental setup used by [79] is shown in Figure 19. Surface roughness was measured using T3110 roughness tester.

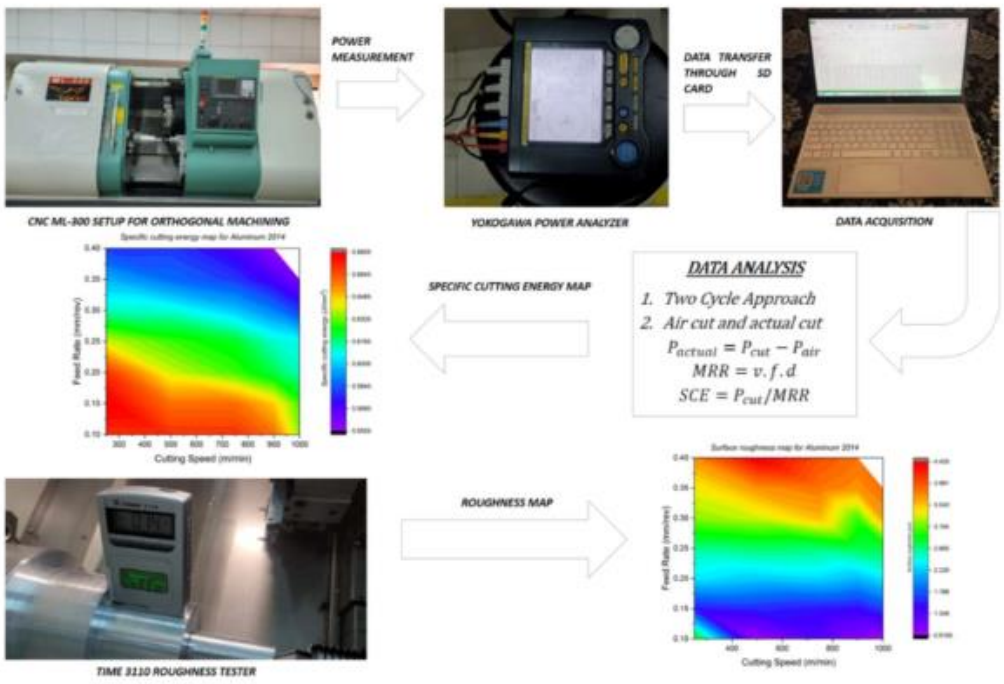

Figure 19: Experimental setup for turning of Al-2014 [79]

The machining parameters used in this study are given in Table 3 and Table 4. Depth of cut was kept constant at 4 mm.

Table 3: Cutting speed used by Shaukat et al., 2023 [79]

Parameter	Level 1	Level 2	Level 3	Level 4	Level 5
v_c (m/min)	250	500	750	900	1000

Table 4: Feed rate used by Shaukat et al., 2023 [79]

Parameter	Level 1	Level 2	Level 3	Level 4	Level 5	Level 6	Level 7
f (mm/rev)	0.1	0.15	0.2	0.25	0.3	0.35	0.4

The roughness results from both [78] and [79] were used to develop a ANN based machine learning model. Training datasets were based on the roughness results turning operations on AISI 4140 and Al-2014, using input features like cutting speed, feed rate, depth of cut, material type, and tool nose radius. Both datasets were preprocessed to ensure consistency, and a speed-squared feature was introduced to capture non-linear relationships.

For data normalization, Min-Max scaling was used to ensure that all the values remained in the range of 0 to 1. An 80-20 philosophy was used for training and validation subsets, respectively. The model architecture was constructed based on a feedforward network using 128 neurons in the input, with 128, 64, and 1 neuron in the hidden layer, respectively. The selection of this internal architecture was done within the model for minimal computational time and highest accuracy. ReLU function was used as an activation function. Additionally, a linear activation function was applied to the output layer. Adam optimizer was utilized to train the network, with an initial learning rate of 0.001, using mean square error (MSE) as the loss function. Training was performed with batch sizes of 16 using 200 epochs. To prevent overfitting, an early stopping strategy was employed. For final testing and validation, the model was tested on completely unseen data, which was not a part of initial dataset used for mode. For good visualization of the trends, results were plotted in the form of contour plots as roughness maps as a function of cutting speed and feed rate. To make the model user-centric, an interactive function was developed asking the user to input feed rate, cutting speed, depth of cut, material type, and tool nose radius, giving an estimation of surface roughness based on the trained model.

5 Results and discussion

Evaluation metrics for the developed ANN model are presented in Table 5. The model was able to develop a strong correlation and predictive reliability, achieving a mean absolute error (MAE) of 0.2208, a mean squared error (MSE) of 0.1123, and an R^2 score of 0.9266. An overall accuracy of 84.21% with the mean absolute percentage error (MAPE) of 15.79% validates the model's capability in accurately estimating surface roughness.

Table 5: Evaluation matrices of the developed ANN model

Parameter	**Value**
Mean absolute error (MAE)	0.2208
Mean squared error (MSE)	0.1123
R^2 score	0.9266
Mean absolute percentage error	15.76%
Accuracy	84.21%

A comparison between actual and predicted roughness values for unseen dataset is presented in Figure 20. The developed ANN model, effectively, captured the nonlinear interactions between the input features and surface roughness. The roughness trend for Al-2014 was closely aligned with the actual values, however, some of the predicted values were a little bit different. However, the predicted trend for AISI 4140 showed minor deviations from actual roughness values. Overall, the model demonstrated a good generalizability.

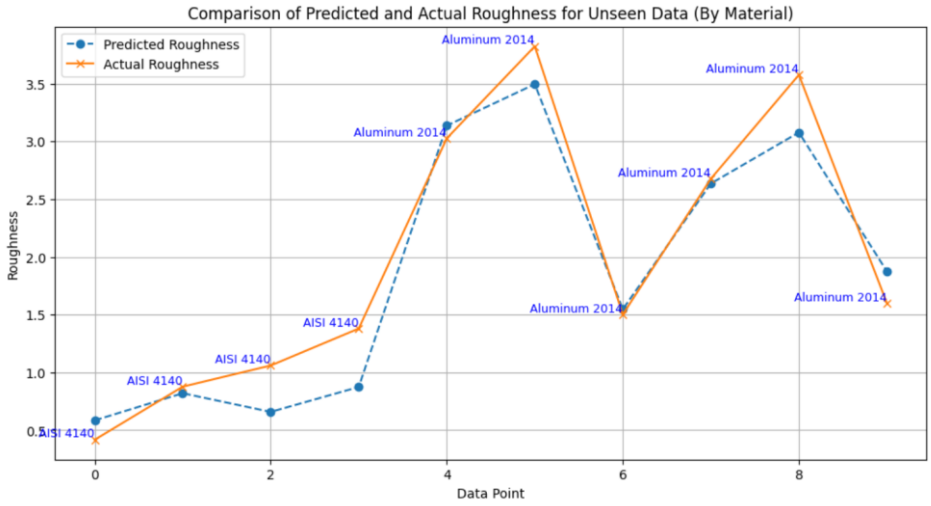

Figure 20: Comparison of predicted and actual surface roughness as predicted by developed ANN model for Al-2014 and AISI 4140

The generated roughness maps for both materials are shown in Figure 21 and Figure 22. From the contour plots, it is visible that surface roughness increased with feed rate, where cutting speed had a varying effect of surface roughness depending on the material. Al-2014 depicted improved surface quality at lower feed rates and moderate cutting speeds. Similar trend was followed by AISI 4140, exhibiting lower surface roughness at lower feed rates and moderate cutting speeds.

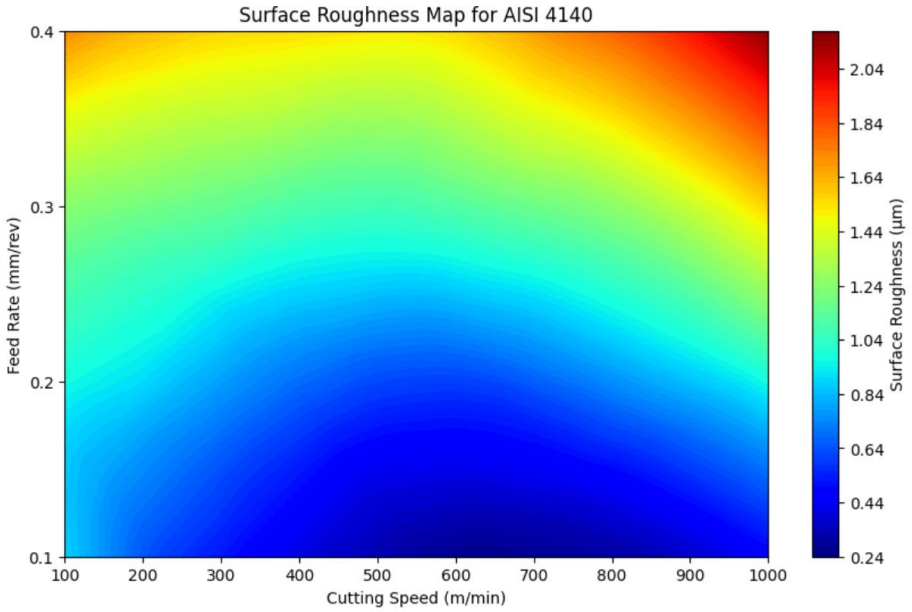

Figure 21: Surface roughness map for AISI 4140

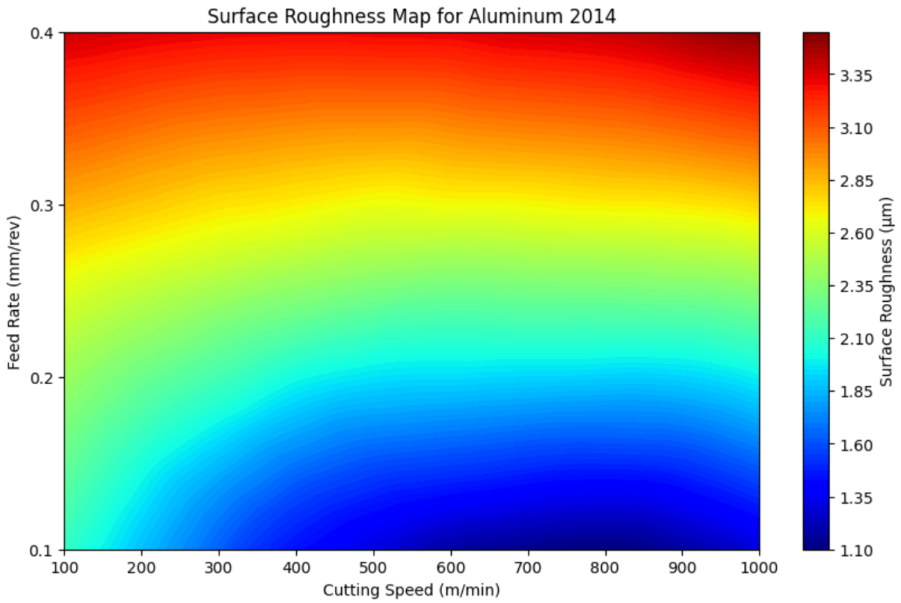

Figure 22: Surface roughness map for Al-2014

6 Conclusions

This study was based on developing an ANN model for predicting surface roughness in machining processes. The developed model demonstrated an accuracy of 84.21%. The findings confirmed that feed rate has the most influential parameter on surface roughness, while cutting speed has a relatively moderate effect. Nonlinear interactions were captured effectively by the ANN model depicting its strong generalizability. However, a noticeable discrepancy was observed in the surface roughness predictions for AISI 4140, suggesting the need for a larger and more diverse dataset which could further enhance the model's predictive accuracy and generalization capability. Further improvements in models can be achieved by the integration of finite element method (FEM) and ML models. This would lead to diverse training data sets, reducing the need for extensive experimentation while improving the ANN model predictive accuracy. Hybrid deep learning techniques like ANN-SVM or transformer-based models, could enhance adaptability and robustness in capturing variables machining conditions. Another possibility is the exploration of utilizing sensors for data acquisition, and then, using it for AI based real time optimization the machining process.

References

[1] Black JT, Kohser RA. Materials and processes in manufacturing. Prentice-Hall International; 1997.
[2] Kalpakjian S, Schmid S. Manufacturing processes for engineering materials–5th edition. Agenda 2014;12:1.
[3] Groover MP. Fundamentals of modern manufacturing materials 2019.
[4] Arrazola PJ, Özel T, Umbrello D, Davies M, Jawahir IS. Recent advances in modelling of metal machining processes. CIRP Ann 2013;62:695–718. https://doi.org/10.1016/j.cirp.2013.05.006.
[5] Mukherjee I, Ray PK. A review of optimization techniques in metal cutting processes. Comput Ind Eng 2006;50:15–34. https://doi.org/10.1016/j.cie.2005.10.001.
[6] Yan J, Li L. Multi-objective optimization of milling parameters – the trade-offs between energy, production rate and cutting quality. J Clean Prod 2013;52:462–71. https://doi.org/10.1016/j.jclepro.2013.02.030.
[7] Li W, Kara S. An empirical model for predicting energy consumption of manufacturing processes: a case of turning process. Proc Inst Mech Eng Part B J Eng Manuf 2011;225:1636–46. https://doi.org/10.1177/2041297511398541.
[8] Draganescu F, Gheorghe M, Doicin CV. Models of machine tool efficiency and specific consumed energy. J Mater Process Technol 2003;141:9–15. https://doi.org/10.1016/S0924-0136(02)00930-5.
[9] Camposeco-Negrete C. Optimization of cutting parameters using Response Surface Method for minimizing energy consumption and maximizing cutting quality in turning of AISI 6061 T6 aluminum. J Clean Prod 2015;91:109–17. https://doi.org/10.1016/j.jclepro.2014.12.017.
[10] Guo Y, Loenders J, Duflou J, Lauwers B. Optimization of Energy Consumption and Surface Quality in Finish Turning. Procedia CIRP 2012;1:512–7. https://doi.org/10.1016/j.procir.2012.04.091.
[11] Baklouti W, Mrad C, Nasri R. Numerical study of the chatter phenomenon in orthogonal turning. Int J Adv Manuf Technol 2018;99:755–64. https://doi.org/10.1007/s00170-018-2528-2.
[12] Davim JP, Davim JP. Modern machining technology: a practical guide. Elsevier; 2011.
[13] Baruah S, Rao BC. A cutting tool architecture designed to address the parasitic mechanisms consuming excess power during machining and manufacturing operations–A review-based study towards sustainable manufacturing. Plos One 2024;19:e0300132.
[14] Shaw M. Metal cutting principles. Clarendon 1984.
[15] Melkote SN, Grzesik W, Outeiro J, Rech J, Schulze V, Attia H, et al. Advances in material and friction data for modelling of metal machining. Cirp Ann 2017;66:731–54.
[16] Lukács J, Horváth R. Comprehensive investigations of cutting with round insert: introduction of a predictive force model with verification. Metals 2022;12:257.
[17] Groover MP. Fundamentals of modern manufacturing: materials, processes, and systems. John Wiley & Sons; 2010.
[18] Piispanen V. Theory of formation of metal chips. J Appl Phys 1948;19:876–81.
[19] Oxley PLB. The mechanics of machining: an analytical approach to assessing machinability. No Title 1989.
[20] Trent EM, Wright PK. Metal cutting. Butterworth-Heinemann; 2000.
[21] Boothroyd G. Fundamentals of metal machining and machine tools. vol. 28. Crc Press; 1988.
[22] Cook NH. Tool wear and tool life 1973.
[23] Loewen EG, Shaw MC. On the analysis of cutting-tool temperatures. Trans Am Soc Mech Eng 1954;76:217–25.
[24] Trigger KJ, Chao BT. An analytical evaluation of metal-cutting temperatures. Trans Am Soc Mech Eng 1951;73:57–66.
[25] Jaeger JC. Moving sources of heat and the temperature at sliding contacts. Proc Roy Soc New South Wales 1942;76:203.
[26] Trigger KJ. Progress Report No. 2 on tool-chip interface temperatures. Trans Am Soc Mech Eng 1949;71:163–70.

[27] Liu H, Meurer M, Bergs T. Modeling and Monitoring of the Tool Temperature During Continuous and Interrupted Turning with Cutting Fluid. Metals 2024;14:1292.
[28] Rani D, Saini K, Hardik, Madan AK. Tool Wear Analysis System based on MATLAB and AI. 2023.
[29] Mali HS, Unune DR. Machinability of Nickel-Based Superalloys: An Overview. Ref. Module Mater. Sci. Mater. Eng., Elsevier; 2017. https://doi.org/10.1016/B978-0-12-803581-8.09817-9.
[30] Adekunle F. Optical Diamond Turning of Rapidly Solidified Aluminium Alloy Grade - 43. 20 n.d.
[31] Vajpayee S. Analytical study of surface roughness in turning. Wear 1981;70:165–75.
[32] Aggogeri F, Pellegrini N, Tagliani FL. Recent advances on machine learning applications in machining processes. Appl Sci 2021;11:8764.
[33] Chopra V, Priyadarshi D. Role of Machine Learning in Manufacturing Sector. Int J Recent Technol Eng IJRTE 2019;8:2320–8. https://doi.org/10.35940/ijrte.D8191.118419.
[34] Khandelwal R. Supervised, Unsupervised and Reinforcement Learning. Lest 2022;21:2024.
[35] Guo M, Wei S, Han C, Xia W, Luo C, Lin Z. Prediction of surface roughness using deep learning and data augmentation. J Intell Manuf Spec Equip 2024;5:221–41.
[36] Kong F, Wang X, Pu K, Zhang J, Dang H. A Practical Non-Profiled Deep-Learning-Based Power Analysis with Hybrid-Supervised Neural Networks. Electronics 2023;12:3361. https://doi.org/10.3390/electronics12153361.
[37] Loaiza K. Deep learning for decision support in dermatology. 2020. https://doi.org/10.13140/RG.2.2.14692.60800.
[38] Wang A, Murdock R, Kauwe S, Oliynyk A, Gurlo A, Brgoch J, et al. Machine Learning for Materials Scientists: An Introductory Guide Towards Best Practices. 2020. https://doi.org/10.26434/chemrxiv.12249752.
[39] Reyad M, Sarhan AM, Arafa M. A modified Adam algorithm for deep neural network optimization. Neural Comput Appl 2023;35:17095–112. https://doi.org/10.1007/s00521-023-08568-z.
[40] Ribeiro J, Tavares S, Parente M. Stress-strain evaluation of structural parts using artificial neural networks. Proc Inst Mech Eng Part J Mater Des Appl 2021. https://doi.org/10.1177/1464420721992445.
[41] Nur R, Noordin M, Izman S, Kurniawan D. Machining parameters effect in dry turning of AISI 316L stainless steel using coated carbide tools. Proc Inst Mech Eng Part E J Process Mech Eng 2017;231:676–83. https://doi.org/10.1177/0954408915624861.
[42] Qehaja N, Jakupi K, Bunjaku A, Bruçi M, Osmani H. Effect of Machining Parameters and Machining Time on Surface Roughness in Dry Turning Process. Procedia Eng 2015;100:135–40. https://doi.org/10.1016/j.proeng.2015.01.351.
[43] Venkata Ramana M, Kumar G. Optimization of Material Removal Rate in Turning of AISI 321 Stainless Steel Using Taguchi Methodology. Mater Today Proc 2018;5:4965–70. https://doi.org/10.1016/j.matpr.2017.12.074.
[44] Tan L, Yao C, Li X, Fan Y, Cui M. Effects of machining parameters on surface integrity when turning Inconel 718. J Mater Eng Perform 2022;31:4176–86.
[45] Wu T-Y, Lin C-C. Optimization of machining parameters in milling process of inconel 718 under surface roughness constraints. Appl Sci 2021;11:2137.
[46] Srivastava VS, Gupta TK, Srivastava AK, Chauhan S, Chauhan PK. Effects of cutting parameters on aluminium alloys-A review. Mater Today Proc 2021;47:3823–7.
[47] Albrecht P. New Developments in the Theory of the Metal-Cutting Process: Part I. The Ploughing Process in Metal Cutting. J Eng Ind 1960;82:348–57. https://doi.org/10.1115/1.3664242.
[48] Thiele JD, N. Melkote S. Effect of cutting edge geometry and workpiece hardness on surface generation in the finish hard turning of AISI 52100 steel. J Mater Process Technol 1999;94:216–26. https://doi.org/10.1016/S0924-0136(99)00111-9.
[49] Childs THC, Dornfeld D, Lee D-E, Min S, Sekiya K, Tezuka R, et al. The influence of cutting edge sharpness on surface finish in facing with round nosed cutting tools. CIRP J Manuf Sci Technol 2008;1:70–5. https://doi.org/10.1016/j.cirpj.2008.09.001.

[50] Childs THC, Sekiya K, Tezuka R, Yamane Y, Dornfeld D, Lee D-E, et al. Surface finishes from turning and facing with round nosed tools. CIRP Ann 2008;57:89–92. https://doi.org/10.1016/j.cirp.2008.03.121.
[51] Daniyan I, Tlhabadira I, Mpofu K, Adeodu A. Investigating the geometrical effects of cutting tool on the surface roughness of titanium alloy (Ti6Al4V) during milling operation. Procedia CIRP 2021;99:157–64.
[52] Saravanamurugan S, Sundar BS, Pranav RS, Shanmugasundaram A. Optimization of cutting tool geometry and machining parameters in turning process. Mater Today Proc 2021;38:3351–7.
[53] Bhushan RK. Effect of tool wear on surface roughness in machining of AA7075/10áwt.% SiC composite. Compos Part C Open Access 2022;8:100254.
[54] Kumar P, Chauhan SR, Aggarwal A. Effects of cutting conditions, tool geometry and material hardness on machinability of AISI H13 using CBN tool. Mater Today Proc 2021;46:9217–22.
[55] Niu Q, Jing L, Li C, Yu Z, Li S, Li P, et al. Study on effects of tool nose radius on the formation mechanism of edge defects during milling SiC p/Al composites. Int J Adv Manuf Technol 2021;114:2261–9.
[56] Wang H, Dong Z, Yuan S, Guo X, Kang R, Bao Y. Effects of tool geometry on tungsten removal behavior during nano-cutting. Int J Mech Sci 2022;225:107384.
[57] Sreejith PS. Machining of 6061 aluminium alloy with MQL, dry and flooded lubricant conditions. Mater Lett 2008;62:276–8. https://doi.org/10.1016/j.matlet.2007.05.019.
[58] Kamata Y, Obikawa T. High speed MQL finish-turning of Inconel 718 with different coated tools. J Mater Process Technol 2007;192–193:281–6. https://doi.org/10.1016/j.jmatprotec.2007.04.052.
[59] Khan MMA, Mithu MAH, Dhar NR. Effects of minimum quantity lubrication on turning AISI 9310 alloy steel using vegetable oil-based cutting fluid. J Mater Process Technol 2009;209:5573–83. https://doi.org/10.1016/j.jmatprotec.2009.05.014.
[60] Javidikia M, Sadeghifar M, Songmene V, Jahazi M. Effect of turning environments and parameters on surface integrity of AA6061-T6: experimental analysis, predictive modeling, and multi-criteria optimization. Int J Adv Manuf Technol 2020;110:2669–83. https://doi.org/10.1007/s00170-020-06027-w.
[61] Gupta MK, Boy M, Korkmaz ME, Yaşar N, Günay M, Krolczyk GM. Measurement and analysis of machining induced tribological characteristics in dual jet minimum quantity lubrication assisted turning of duplex stainless steel. Measurement 2022;187:110353.
[62] Shinge VR, Pable MJ. Effect of nano-minimum quantity lubrication on cutting temperature and surface roughness of milling AISI D3 tool steel. Mater Today Proc 2023;72:1758–64.
[63] Kumari S, Shah M, Modi Y, Bandhu D, Zadafiya K, Abhishek K, et al. Effect of various lubricating strategies on machining of titanium alloys: A state-of-the-art review. Coatings 2022;12:1178.
[64] Zhang L, Zhang X. Effect of cooling and lubrication conditions on the variable angle milling of unidirectional CFRP with PCD tools. J Mater Process Technol 2023;319:118073.
[65] Değirmenci Ü, Usca ÜA, Şap S. Machining characterization and optimization under different cooling/lubrication conditions of Al-4Gr hybrid composites fabricated by vacuum sintering. Vacuum 2023;208:111741.
[66] Şap S, Usca ÜA, Uzun M, Kuntoğlu M, Salur E, Pimenov DY. Investigation of the effects of cooling and lubricating strategies on tribological characteristics in machining of hybrid composites. Lubricants 2022;10:63.
[67] Chauhan D, Makhesana MA, Rahman Rashid RA, Joshi V, Khanna N. Comparison of machining performance of Ti-6Al-4V under dry and cryogenic techniques based on tool wear, surface roughness, and power consumption. Lubricants 2023;11:493.
[68] Singh R, Sharma V. Machining induced surface integrity behavior of nickel-based superalloy: effect of lubricating environments. J Mater Process Technol 2022;307:117701.
[69] Danish M, Gupta MK, Rubaiee S, Ahmed A, Korkmaz ME. Influence of hybrid Cryo-MQL lubri-cooling strategy on the machining and tribological characteristics of Inconel 718. Tribol Int 2021;163:107178.

[70] Liu F, Wu X, Xia Y, Lv T, Zhang R, Hu X, et al. A novel cold air electrostatic minimum quantity lubrication (CAEMQL) technique for the machining of titanium alloys Ti–6Al–4 V. Int J Adv Manuf Technol 2023;126:3437–52.
[71] Pimenov DY, Mia M, Gupta MK, Machado ÁR, Pintaude G, Unune DR, et al. Resource saving by optimization and machining environments for sustainable manufacturing: A review and future prospects. Renew Sustain Energy Rev 2022;166:112660.
[72] Yang H, Zheng H, Zhang T. A review of artificial intelligent methods for machined surface roughness prediction. Tribol Int 2024:109935.
[73] Motta MP, Pelaingre C, Delameziere A, Ayed LB, Barlier C. Machine learning models for surface roughness monitoring in machining operations. Procedia CIRP 2022;108:710–5.
[74] Mazid AM, Imam T, Ahsan KB, Khandoker N. Characterising surface roughness of Ti-6Al-4V alloy machined using coated and uncoated carbide tools with variable nose radius by machine learning. Eng Appl Artif Intell 2023;124:106546.
[75] Eser A, Aşkar Ayyıldız E, Ayyıldız M, Kara F. Artificial Intelligence-Based Surface Roughness Estimation Modelling for Milling of AA6061 Alloy. Adv Mater Sci Eng 2021;2021:5576600.
[76] Ross NS, Mashinini PM, Shibi CS, Gupta MK, Korkmaz ME, Krolczyk GM, et al. A new intelligent approach of surface roughness measurement in sustainable machining of AM-316L stainless steel with deep learning models. Measurement 2024;230:114515.
[77] Huang PB, Inderawati MMW, Rohmat R, Sukwadi R. The development of an ANN surface roughness prediction system of multiple materials in CNC turning. Int J Adv Manuf Technol 2023;125:1193–211.
[78] Laakso SVA, Mityakov A, Niinimäki T, Ribeiro KSB, Bessa WM. Hybrid FE-ML model for turning of 42CrMo4 steel. CIRP J Manuf Sci Technol 2024;55:333–46.
[79] Shaukat U, Gohari S, Molla T. Energy consumption and surface roughness maps for low and moderate speed machining of Aluminum alloy 2014: An experimental study. AIMS Mater Sci 2023;10.

Appendix

Step 1: ANN Model

```
import pandas as pd
import numpy as np
from sklearn.preprocessing import MinMaxScaler
from sklearn.model_selection import train_test_split
from tensorflow.keras.models import Sequential
from tensorflow.keras.layers import Dense, Dropout
from tensorflow.keras.optimizers import Adam
from tensorflow.keras.callbacks import EarlyStopping, ReduceLROnPlateau, Callback
from sklearn.metrics import mean_absolute_error, mean_squared_error, r2_score
import matplotlib.pyplot as plt

# Step 1: Custom callback to stop training at a specific learning rate
class StopAtLearningRate(Callback):
    def __init__(self, min_lr=1.25e-04):
        super(StopAtLearningRate, self).__init__()
        self.min_lr = min_lr

    def on_epoch_end(self, epoch, logs=None):
        current_lr = float(self.model.optimizer.learning_rate.numpy())
        if current_lr <= self.min_lr:
            print(f"\nStopping training as learning rate has reached {current_lr:.5e}")
            self.model.stop_training = True

# Step 2: Load and preprocess the datasets
# AISI 4140 Training Data
aisi_data = pd.read_csv("AISI_4140_training_data.csv", delimiter=';', decimal=',', skiprows=[0])
aisi_data.columns = ['Speed', 'Feed Rate', 'Depth of Cut', 'Roughness']
aisi_data['Material'] = 0  # AISI 4140 = 0
aisi_data['Nose Radius'] = 0.8  # Nose radius for AISI 4140

# Aluminum 2014 Training Data
aluminum_data = pd.read_csv("Aluminum_2014_training_data.csv", delimiter=';', decimal=',',
skiprows=[0])
```

```
aluminum_data.columns = ['Feed Rate', 'Speed', 'Depth of Cut', 'Roughness']
aluminum_data['Material'] = 1  # Aluminum 2014 = 1
aluminum_data['Nose Radius'] = 0.387  # Nose radius for Aluminum 2014

# Combine datasets
combined_data = pd.concat([aisi_data, aluminum_data], ignore_index=True)

# Feature engineering
combined_data['Speed^2'] = combined_data['Speed'] ** 2

# Step 3: Separate features and target
X = combined_data[['Feed Rate', 'Speed', 'Depth of Cut', 'Speed^2', 'Material', 'Nose Radius']].values
y = combined_data['Roughness'].values

# Step 4: Scale the features and target
scaler_x = MinMaxScaler()
scaler_y = MinMaxScaler()
X_scaled = scaler_x.fit_transform(X)
y_scaled = scaler_y.fit_transform(y.reshape(-1, 1))

# Step 5: Train/test split
X_train, X_val, y_train, y_val = train_test_split(X_scaled, y_scaled, test_size=0.2, random_state=42)

# Step 6: Build and train the ANN model
def build_and_train_ann(X_train, y_train, X_val, y_val):
    model = Sequential()
    model.add(Dense(128, activation='relu', input_dim=X_train.shape[1]))
    model.add(Dense(128, activation='relu'))
    model.add(Dropout(0.3))
    model.add(Dense(64, activation='relu'))
    model.add(Dense(1, activation='linear'))

    # Compile the model
    optimizer = Adam(learning_rate=0.001)
    model.compile(optimizer=optimizer, loss='mean_squared_error')
```

```
    # Callbacks
    early_stopping = EarlyStopping(monitor='val_loss', patience=20, restore_best_weights=True)
    lr_scheduler = ReduceLROnPlateau(monitor='val_loss', factor=0.5, patience=10, verbose=1)
    stop_at_lr = StopAtLearningRate(min_lr=1.25e-04)  # Stop when learning rate <= 1.2500e-04

    # Train the model
    history = model.fit(
        X_train, y_train,
        validation_data=(X_val, y_val),
        epochs=200,
        batch_size=16,
        callbacks=[early_stopping, lr_scheduler, stop_at_lr],
        verbose=1
    )
    return model, history

model, history = build_and_train_ann(X_train, y_train, X_val, y_val)

# Step 7: Predict on unseen data
# AISI 4140 Unseen Data
aisi_unseen = np.array([
    [0.075, 225, 0.3, 225**2, 0, 0.8],
    [0.075, 135, 0.3, 135**2, 0, 0.8],
    [0.15, 270, 0.6, 270**2, 0, 0.8],
    [0.15, 90, 0.6, 90**2, 0, 0.8]
])

# Aluminum 2014 Unseen Data
aluminum_unseen = np.array([
    [0.3, 900, 4, 900**2, 1, 0.387],
    [0.35, 750, 4, 750**2, 1, 0.387],
    [0.15, 900, 4, 900**2, 1, 0.387],
    [0.25, 750, 4, 750**2, 1, 0.387],
    [0.3, 750, 4, 750**2, 1, 0.387],
    [0.15, 500, 4, 500**2, 1, 0.387]
])
```

```
# Combine unseen data
unseen_data = np.vstack([aisi_unseen, aluminum_unseen])
unseen_scaled = scaler_x.transform(unseen_data)

# Predict roughness
predicted_roughness_scaled = model.predict(unseen_scaled)
predicted_roughness = scaler_y.inverse_transform(predicted_roughness_scaled)

# Step 8: Actual roughness values
actual_roughness_aisi = [0.4167, 0.8767, 1.0600, 1.3800]  # AISI 4140 actual values
actual_roughness_aluminum = [3.0275, 3.825, 1.5025, 2.6775, 3.5775, 1.6]  # Aluminum 2014 actual values
actual_roughness = np.array(actual_roughness_aisi + actual_roughness_aluminum)

# Step 9: Evaluation metrics
y_pred = model.predict(X_scaled)
y_pred_original = scaler_y.inverse_transform(y_pred)
y_original = scaler_y.inverse_transform(y_scaled)

mae = mean_absolute_error(y_original, y_pred_original)
mse = mean_squared_error(y_original, y_pred_original)
r2 = r2_score(y_original, y_pred_original)
mape = np.mean(np.abs((y_original - y_pred_original) / np.abs(y_original))) * 100
accuracy = 100 - mape

print("\nEvaluation Metrics for Combined Model:")
print(f"Mean Absolute Error (MAE): {mae:.4f}")
print(f"Mean Squared Error (MSE): {mse:.4f}")
print(f"R² Score: {r2:.4f}")
print(f"Mean Absolute Percentage Error (MAPE): {mape:.2f}%")
print(f"Accuracy: {accuracy:.2f}%")

# Step 10: Plot predicted vs actual roughness for unseen data
plt.figure(figsize=(12, 6))
plt.plot(predicted_roughness, label='Predicted Roughness', marker='o', linestyle='--')
```

```
plt.plot(actual_roughness, label='Actual Roughness', marker='x', linestyle='-')
material_labels = ['AISI 4140'] * len(actual_roughness_aisi) + ['Aluminum 2014'] *
len(actual_roughness_aluminum)
for i, label in enumerate(material_labels):
    plt.text(i, actual_roughness[i], label, fontsize=9, ha='right', va='bottom', color='blue')  # Add labels
to the plot
plt.title('Comparison of Predicted and Actual Roughness for Unseen Data (By Material)')
plt.ylabel('Roughness')
plt.xlabel('Data Point')
plt.legend()
plt.grid(True)
plt.show()

# Print actual vs predicted values with material labels
print("\nComparison of Actual and Predicted Roughness with Materials:")
for i, (material, actual, predicted) in enumerate(zip(material_labels, actual_roughness,
predicted_roughness.flatten())):
    print(f"Data Point {i + 1}: Material = {material}, Actual Roughness = {actual:.4f}, Predicted
Roughness = {predicted:.4f}")

# Step 11: Generate roughness maps for both materials
# Define the range of Cutting Speed and Feed Rate for the map
speed_range = np.linspace(100, 1000, 100)  # Cutting speed (m/min)
feed_rate_range = np.linspace(0.1, 0.4, 100)  # Feed rate (mm/rev)

# Create a grid of Cutting Speed and Feed Rate values
speed_grid, feed_rate_grid = np.meshgrid(speed_range, feed_rate_range)

# Material-specific parameters
depth_of_cut = 0.3  # Example fixed depth of cut
nose_radius_aisi = 0.8  # AISI 4140 nose radius
nose_radius_aluminum = 0.387  # Aluminum 2014 nose radius

# Flatten the grids to prepare for prediction
speed_flat = speed_grid.flatten()
feed_rate_flat = feed_rate_grid.flatten()
```

```
# Prepare data for AISI 4140
data_aisi = np.array([
    [feed_rate, speed, depth_of_cut, speed**2, 0, nose_radius_aisi]
    for feed_rate, speed in zip(feed_rate_flat, speed_flat)
])

# Prepare data for Aluminum 2014
data_aluminum = np.array([
    [feed_rate, speed, depth_of_cut, speed**2, 1, nose_radius_aluminum]
    for feed_rate, speed in zip(feed_rate_flat, speed_flat)
])

# Scale the input data
data_aisi_scaled = scaler_x.transform(data_aisi)
data_aluminum_scaled = scaler_x.transform(data_aluminum)

# Predict roughness
roughness_aisi_scaled = model.predict(data_aisi_scaled)
roughness_aluminum_scaled = model.predict(data_aluminum_scaled)

# Inverse-transform the predictions to get roughness in original units
roughness_aisi = scaler_y.inverse_transform(roughness_aisi_scaled).reshape(speed_grid.shape)
roughness_aluminum =
scaler_y.inverse_transform(roughness_aluminum_scaled).reshape(speed_grid.shape)

# Plot roughness map for AISI 4140
plt.figure(figsize=(10, 6))
contour_aisi = plt.contourf(speed_grid, feed_rate_grid, roughness_aisi, levels=100, cmap='jet')
plt.colorbar(contour_aisi, label='Surface Roughness (μm)')
plt.title('Surface Roughness Map for AISI 4140')
plt.xlabel('Cutting Speed (m/min)')
plt.ylabel('Feed Rate (mm/rev)')
plt.yticks(np.linspace(0.1, 0.4, 4))  # Correct feed rate ticks: 0.1, 0.2, 0.3, 0.4
plt.show()
```

```
# Plot roughness map for Aluminum 2014
plt.figure(figsize=(10, 6))
contour_aluminum = plt.contourf(speed_grid, feed_rate_grid, roughness_aluminum, levels=100,
cmap='jet')
plt.colorbar(contour_aluminum, label='Surface Roughness (μm)')
plt.title('Surface Roughness Map for Aluminum 2014')
plt.xlabel('Cutting Speed (m/min)')
plt.ylabel('Feed Rate (mm/rev)')
plt.yticks(np.linspace(0.1, 0.4, 4))  # Correct feed rate ticks: 0.1, 0.2, 0.3, 0.4
plt.show()
```

Step 2: Function to be called

```
def predict_roughness_debug(speed, feed_rate, depth_of_cut, material, nose_radius, model, scaler_x,
scaler_y):
    """
    Predict roughness using the trained model with minimal input.

    Parameters:
        speed (float): Cutting speed.
        feed_rate (float): Feed rate.
        depth_of_cut (float): Depth of cut.
        material (int): Material type (0 for AISI 4140, 1 for Aluminum 2014).
        nose_radius (float): Nose radius of the tool.
        model: The trained ANN model.
        scaler_x: Scaler used to normalize features during training.
        scaler_y: Scaler used to normalize target values during training.

    Returns:
        Predicted roughness (float).
    """
    # Calculate Speed^2
    speed_squared = speed ** 2

    # Create input data array
    new_data = np.array([[feed_rate, speed, depth_of_cut, speed_squared, material, nose_radius]])
```

```
    # Scale the input features
    scaled_data = scaler_x.transform(new_data)
    print("Scaled Input Data:", scaled_data)  # Debugging scaled data

    # Predict using the model
    raw_prediction = model.predict(scaled_data)
    print("Raw Prediction (Scaled):", raw_prediction)  # Debugging raw output

    # Inverse-transform the predictions
    predicted_roughness = scaler_y.inverse_transform(raw_prediction)
    print("Inverse Transformed Prediction:", predicted_roughness)  # Debugging inverse-transformed
output

    return predicted_roughness[0][0]  # Return the single predicted roughness value
```

Step 3: Calling the fucntion

```
# Just enter the input values
speed = 250  # Cutting speed
feed_rate = 0.225  # Feed rate
depth_of_cut = 4  # Depth of cut
material = 1  # 0 for AISI 4140, 1 for Aluminum 2014
nose_radius = 0.387  # Nose radius for the given tool 0.387 or 0.8

# Call the function
predicted_roughness = predict_roughness_debug(speed, feed_rate, depth_of_cut, material,
nose_radius, model, scaler_x, scaler_y)

# Print the result
print(f"Predicted Roughness: {predicted_roughness:.4f}")
```